

# The number of cosmic string loops

Jose J. Blanco-Pillado,<sup>1,2,3</sup> Ken D. Olum,<sup>3</sup> and Benjamin Shlaer<sup>3</sup>

<sup>1</sup>*Department of Theoretical Physics,*

*University of the Basque Country, 48080, Bilbao, Spain*

<sup>2</sup>*IKERBASQUE, Basque Foundation for Science, 48011, Bilbao, Spain*

<sup>3</sup>*Institute of Cosmology, Department of Physics and Astronomy,  
Tufts University, Medford, MA 02155, USA*

## Abstract

Using recent simulation results, we provide the mass and speed spectrum of cosmic string loops. This is the quantity of primary interest for many phenomenological signatures of cosmic strings, and it can be accurately predicted using recently acquired detailed knowledge of the loop production function. We emphasize that gravitational smoothing of long strings does not play any role in determining the total number of existing loops. We derive a bound on the string tension imposed by recent constraints on the stochastic gravitational wave background from pulsar timing arrays, finding  $G\mu \leq 2.8 \times 10^{-9}$ . We also provide a derivation of the Boltzmann equation for cosmic string loops in the language of differential forms.

## CONTENTS

I. Introduction	2
II. Cosmic string loop production and decay	4
A. Scaling of loops	4
B. Radiation era	6
C. Matter era	11
D. Loops surviving from the radiation era	16
III. Stochastic gravitational waves and a bound on $G\mu$	18
IV. Conclusions	22
Acknowledgments	24
A. Differential forms	24
1. Introduction	24
2. The Boltzmann equation	25
3. The flow $(M, P)$	26
4. The solution	27
B. The exact flow	28
C. Tiny, recent loops	29
References	31

## I. INTRODUCTION

A longstanding problem in the theory of cosmic strings is how to predict the distribution of loops that exist at any given time. This distribution provides the input for calculations of many observable effects. For example, stochastic gravitational wave signals [1–14] as well as bursts [15–20] are proportional to the number of loops above a critical size dependent on the frequency band of the detector. The ionization history of the universe is affected by loops through early star formation [21, 22], which is seeded by the large, slow loops. Neutral hydrogen overdensities caused by loops [23, 24] create bright spots in high-redshift 21cm surveys, and dark matter overdensities [25] have enhanced decay signatures. Microlensing of stars may occur from loops slow enough to be captured by galaxy halos, even for very low tensions [26–28]. Magnetogenesis on galactic scales [29] may be aided by large cosmic string loops. Cosmic rays from ordinary [30–35] and superconducting cosmic strings [36–40] are emitted via cusps and kinks on loops. Additional couplings of the string to other degrees of freedom could also lead to other forms of radiation by loops [41–47].

Our goal here is to provide a definitive description of the number density of loops of a given size and velocity, based on recent simulations [48, 49]. Simulations give us the rate of production of the loops over the timescale of the simulations. We then extrapolate these results and embed them in a cosmological context. While the simulations have not yet determined the production rate of loops that are very small relative to the horizon

size, the production of larger loops is reasonably well agreed upon. As we will show, the uncertainty about the production of tiny loops is of no consequence for any known observable effect, because small loops produced recently are dwarfed by loops of the same (current) size produced long ago, when the string network (and the universe) were much more dense.

The reason that it is possible to extrapolate from simulations, which can cover only a few orders of magnitude in the growth of the universe, to cosmological phenomenology is the *scaling* nature of cosmic string networks; there is only one kinematic scale, which we take to be the horizon distance, and all other length scales, such as the Hubble length, are proportional to the horizon distance. By understanding the self-similar dynamics numerically, we can extrapolate the network behavior through all cosmological epochs.

Scaling of the loop distribution means that the number of loops of a given fraction of the horizon size contained in a single horizon volume should not change with time, once the scaling distribution is established. The earliest work [50, 51] seemed to indicate a scaling distribution, but subsequent numerical simulations [52–55] found instead that most energy went to loops at the minimum resolution allowed in the simulations, rather than scaling with the horizon size. Extrapolating those results in a cosmological context, one would conclude that loops are always produced at a scale determined by gravitational back-reaction, since this is smallest relevant scale.

The question then arose [56, 57] whether the simulation-resolution loops represented a real feature of a cosmic string network or were rather an artifact of the initial conditions. Indeed, more recent simulations have determined that a significant fraction of loops are produced at scales roughly a few orders of magnitude below the horizon size, after a transient initial regime. In Ringeval, Sakellariadou, and Bouchet [57] (hereafter RSB), a scaling sub-population of large loops was first shown to exist over a range of sizes within a few orders of magnitude of the horizon scale. Subsequently, Refs. [48, 58, 59] found scaling in the rate of production of loops, rather than the distribution of existing loops. Although slightly different definitions<sup>1</sup> were used, the phenomenological results are in agreement, namely that the spectrum of loops in horizon units is set by a scale of order unity, rather than the gravitational smoothing scale. The most recent simulation [48] found scaling of the loop production function over five orders of magnitude in loop size, which is enough to determine the loop distribution to within a few percent. The agreement between [48] and [57] is rather good in both the radiation and matter eras, as our figures will show.

Reference [60] is not directly comparable with this paper, since an analytic model of loop production was used to bridge the gap between simulation data for horizon-scale loops, and the gravitational back-reaction scale. Their analytic model assumes most loops were produced at the gravitational back-reaction scale, and hence differs quite significantly from our simulated loop production function. In particular, we find that the vast majority of loops existing at any given time were produced with a size within a few orders of magnitude of the horizon size at the time of production.

An important consideration which has not been widely appreciated is the speed of loops emitted from the network [61]. Small loops are created with ultra-relativistic speeds, and thus lose most of their energy to redshifting. Except for loops so small that they decay within a few Hubble times, it is better to classify loops by their rest mass (i.e., the total energy of a loop viewed in the frame where the center of mass is at rest). We find that a negligible fraction of mass is injected into loops well below the horizon size. Thus, it is loops

---

<sup>1</sup> Refs. [48, 59] only considered loops on non-self-intersecting trajectories, while RSB considered any closed string shorter than the horizon to be a loop.

produced within a few orders of magnitude of the horizon size that account for most of the loops of any given size that exist at any given time.

Large loops are emitted with velocities on the order of 0.3, where we assume the speed of light is unity throughout. In terms of Lorentz boost, this is of little consequence, but if one is concerned with seeding structure formation [22] or capture of small loops in galaxies [27], even non-relativistic velocities are important.

## II. COSMIC STRING LOOP PRODUCTION AND DECAY

### A. Scaling of loops

Simulations have revealed that the long strings in a cosmic string network obey a scaling solution [48, 50–55, 57–59, 62]. We will describe all scaling quantities using the horizon distance  $d_h$ , which in a radiation dominated or matter dominated universe is related to cosmic time  $t$  by  $d_h = 2t$  or  $d_h = 3t$ , respectively. We will specify the comoving loop production function as a function<sup>2</sup>  $f(t, m, p)$ , where  $t$  is the time of production,  $m$  the rest mass of the loop, and  $p$  is the momentum per unit mass, i.e.,  $p = v\gamma = v/\sqrt{1-v^2}$ , where  $v$  is the center-of-mass velocity of the loop and  $\gamma$  is its Lorentz boost. We will sometimes refer to  $p$  as just the momentum. Then  $f(t, m, p)dt dm dp$  gives the number of loops produced per comoving volume in time interval  $dt$  with rest mass between  $m$  and  $m + dm$  and momentum per unit mass between  $p$  and  $p + dp$ .

We define true scaling when not just the normalization, but also the shape of the spectrum of power flowing into loops becomes time-independent when  $m$  is expressed in units of  $\mu d_h$ . Thus we define a scaling measure of the loop mass

$$\alpha = \frac{m}{d_h \mu}, \quad (1)$$

and a scaling loop production function  $f(\alpha, p)$ , so that  $f(\alpha, p)d\alpha dp$  is essentially the number of loops produced in volume  $d_h^3$  in time  $d_h$  with  $\alpha$  and  $p$  in a range of size  $d\alpha$  and  $dp$ . More precisely,

$$\frac{f(\alpha, p)}{d_h^4} = \frac{f(t, m, p)}{a^3} \frac{\partial m}{\partial \alpha}, \quad (2)$$

where  $\partial m/\partial \alpha = \mu d_h$  is the Jacobian determinant for changing coordinates from  $m$  to  $\alpha$ . Hence,

$$f(\alpha, p) = \frac{\mu d_h^5}{a^3} f(t, m, p). \quad (3)$$

Numerical evidence now exists that the loop production power will eventually scale<sup>3</sup>.

We characterize the distribution of cosmic string loops at time  $t$  by  $n(t, m, p)dm dp$ , the comoving number density of loops of rest mass between  $m$  and  $m + dm$  and momentum

<sup>2</sup> Such quantities can more elegantly be described in the language of differential forms. See Appendix A.

<sup>3</sup> In fact, numerical simulations to date have only shown that large loop power scales, and that the majority of power is flowing into small loops not yet proven to scale. We will see that enough large loop production has been found that the fate of these small loops is immaterial for the purposes of calculating the number density of loops  $n$ , although we believe small loop power does eventually scale, even in the absence of gravitational backreaction. We no longer [48] believe that the large loop portion of  $f$  will be significantly affected by this.

per unit mass between  $p$  and  $p + dp$ . The scaling number density distribution is given by  $n(\alpha, p)d\alpha dp$ , the number of loops in volume  $d_h^3$  whose  $\alpha$  and  $p$  are in ranges of size  $d\alpha$  and  $dp$ . The two functions are related by

$$n(\alpha, p) = \frac{\mu d_h^4}{a^3} n(t, m, p). \quad (4)$$

The loop distribution can be determined by integrating the loop production function. (We assume that strings were formed early enough that no loop present at the time of string formation could survive to any time of interest.) The number of loops in a given comoving volume at time  $t$  with  $m$  and  $p$  in given ranges is just the total number of loops produced at all earlier times whose mass and momentum will, after evolving to time  $t$ , fall in the given ranges. Thus

$$n(t, m, p) = \int_0^t f(t', M', P') \frac{\partial M'}{\partial m} \frac{\partial P'}{\partial p} dt', \quad (5)$$

where  $M'$  and  $P'$  are the mass and momentum at time  $t'$  of a loop which will eventually have mass  $m$  and momentum  $p$  at time  $t$ .<sup>4</sup>

Loops oscillate and decay by emission of gravitational radiation, and the momentum of a loop decreases with the expansion of the universe. We will neglect the change of the momentum due to gravitational wave emission, the so-called ‘‘rocket effect’’, and consider only redshifting, so the momentum is just inversely proportional to the scale factor,

$$P' = p \frac{a}{a'}, \quad (6)$$

and so  $\partial P'/\partial p = a/a'$ . A more careful treatment is necessary if one wishes to consider the effects of very slow loops, e.g., gravitational clustering [26, 27].

The rate of gravitational radiation from a loop does not depend on its size. Thus a loop that was slightly more massive than another at production will be the same amount more massive today, and thus

$$\frac{\partial M'}{\partial m} = 1. \quad (7)$$

Putting Eqs. (6) and (7) in Eq. (5) we find

$$n(t, m, p) = \int_0^t f(t', M', P') \frac{a}{a'} dt', \quad (8)$$

which in scaling coordinates becomes

$$n(\alpha, p) = \int_0^t \frac{a'^2}{a^2} \frac{d_h^4}{d_h^5} f(\alpha', P') dt', \quad (9)$$

where  $\alpha' = M'/(d_h' \mu)$ .

---

<sup>4</sup> The quantities  $M'$  and  $P'$  depend on the time of production,  $t'$ , and also on the loop parameters of interest,  $m$  and  $p$ , and the time  $t$  at which it has those parameters. We can write them as functions  $M' = M(t'; t, m, p)$  and  $P' = P(t'; t, m, p)$ . These functions define the *flow*, which, along with Eq. (5), is derived more formally in Appendix A. Here and below, we use capital symbols to indicate solutions to the flow, and primed symbols indicate that the suppressed time argument is  $t'$ , rather than  $t$ .

We can change variables and integrate over the scaling mass of the loop at production, rather than the time of production to get

$$n(\alpha, p) = \int_{\infty}^{\alpha} \frac{a'^2}{a^2} \frac{d_h^4}{d_h'^5} f\left(\alpha', p \frac{a}{a'}\right) \frac{\partial t'}{\partial \alpha'} d\alpha'. \quad (10)$$

For most purposes, as we will discuss, it is sufficient to consider only nonrelativistic center-of-mass speeds. In that case, the change of mass is given by the gravitational radiation power  $\Gamma G\mu^2$  without accounting for time dilation, so

$$M' \approx m + \Gamma G\mu^2 (t - t'), \quad (11)$$

where  $\Gamma$  is a number of order 50–100. The exact flow of the mass is given in Appendix B.

In a radiation or matter dominated universe, we can write the scale factor  $a \propto t^\nu$ , and thus  $d_h = t/(1-\nu)$ , with  $\nu = 1/2$  for radiation and  $\nu = 2/3$  for matter. Thus using Eq. (11) we find

$$\frac{t'}{t} = \frac{\alpha + (1-\nu)\Gamma G\mu}{\alpha' + (1-\nu)\Gamma G\mu}, \quad (12)$$

and so

$$n(\alpha, p) = \frac{(1-\nu) \int_{\alpha}^{\infty} (\alpha' + (1-\nu)\Gamma G\mu)^{3-2\nu} f\left(\alpha', p \frac{a}{a'}\right) d\alpha'}{(\alpha + (1-\nu)\Gamma G\mu)^{4-2\nu}}, \quad (13)$$

with

$$\frac{a}{a'} p = \left(\frac{t}{t'}\right)^\nu p = \left(\frac{\alpha' + (1-\nu)\Gamma G\mu}{\alpha + (1-\nu)\Gamma G\mu}\right)^\nu p. \quad (14)$$

In most cases we will not be very sensitive to the precise speed of the loops, so we can integrate over  $p$  to get the density of loops without regard to momentum,

$$n(\alpha) = \frac{(1-\nu) \int_{\alpha}^{\infty} (\alpha' + (1-\nu)\Gamma G\mu)^{3-3\nu} f(\alpha') d\alpha'}{(\alpha + (1-\nu)\Gamma G\mu)^{4-3\nu}}, \quad (15)$$

where we have defined  $f(\alpha) = \int_0^{\infty} f(\alpha, p) dp$ .

## B. Radiation era

We show in Fig. 1 the rate of mass produced in cosmic string loops from 8 radiation-era simulations in a box of size 1500 initial correlation lengths with starting conformal time 6, ending time 1506 and thus dynamic range 251. For details on the simulation procedure see Refs. [48, 49]. For large loops, the Lorentz boost is typically small, around 1.1, but for very small loops it is quite high. (This happens because the string is sufficiently smooth at small scales that the only way for small loops to be emitted is for the underlying string to be highly contracted and boosted.) As a result, the non-scaling peak in mass production at small  $\alpha$  (scaling mass) is much smaller than the non-scaling energy production peak at small  $x$  (scaling energy) shown in Ref. [48].

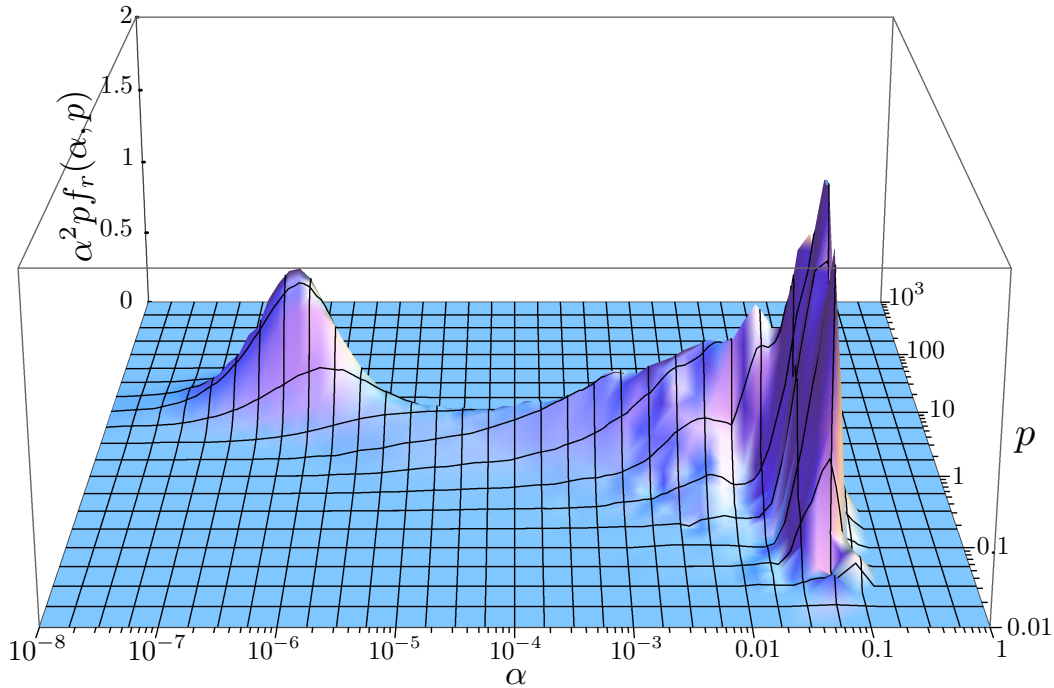


FIG. 1. The scaling rate of mass flowing into cosmic string loops in a radiation dominated universe simulation. The spectrum is given in logarithmic bins of scaling mass  $\alpha = m/(\mu d_h)$  and momentum/mass  $p = v/\sqrt{1-v^2}$ . The vertical axis,  $\alpha^2 p f_r(\alpha, p)$ , is chosen so that the volume under the surface gives the total mass flow. (This effect is described more fully in Appendix A.) The peak at  $\alpha \sim 10^{-6}$  is non-scaling, an artifact of the resolution of initial conditions. This error is a subdominant total mass fraction flowing into loops, but as visible in Ref. [48], it is a dominant energy fraction, due to very large speeds of small loops. We will show that this artifact has no effect on the spectrum of loops  $n(\alpha)$ .

We can disregard momenta and find the distribution of loops by mass alone using Eq. (15) with  $\nu = 1/2$ ,

$$n_r(\alpha) = \frac{\int_{\alpha}^{\infty} (\alpha' + \Gamma G\mu/2)^{3/2} f_r(\alpha') d\alpha'}{2(\alpha + \Gamma G\mu/2)^{5/2}}. \quad (16)$$

Let us look first at the numerator. If gravitational effects can be neglected, it is just  $\int_{\alpha}^{\infty} \alpha'^{3/2} f_r(\alpha') d\alpha'$ . We plot the integrand in Fig. 2. There is an extra half power of  $\alpha'$  relative to Fig. 1. It appears because the energy density in loops is only diluted as  $1/a^3$ , whereas the network is putting energy into loops as  $1/a^4$ . Thus the network produces many more loops at early times, when the network density is higher, so large loops from early times are more numerous than loops of identical physical size produced later on, despite dilution from the intervening expansion. As a result of this extra half power, the dominant contribution to loops of any scaling mass  $\alpha$  comes from production of large loops, and the peak at small scales gives no significant contribution; for any realistic  $G\mu$ , loops with  $\alpha' \sim \Gamma G\mu$  give no substantial contribution, as shown in Fig. 2. Thus, even though we do not know the eventual fate of the small-scale peak, that uncertainty does not yield any important uncertainty in the resulting  $n(\alpha)$ .

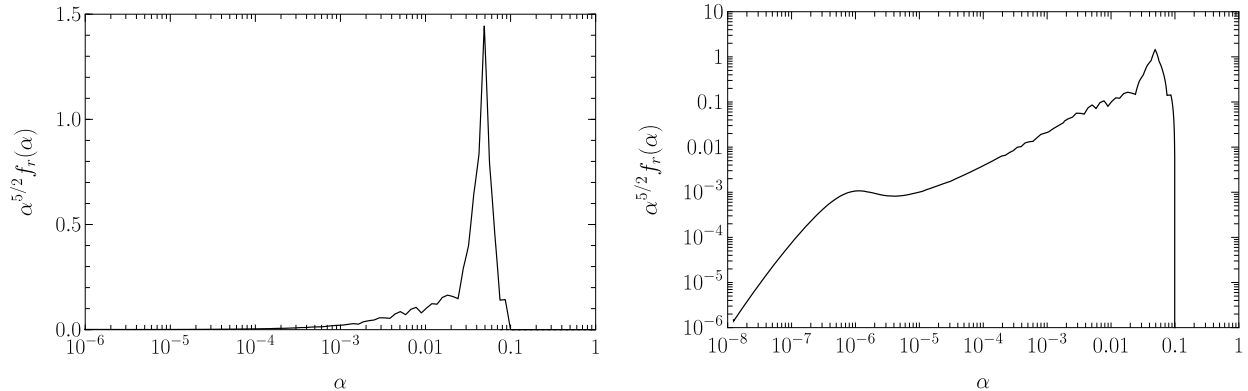


FIG. 2. The loop production rate  $f_r(\alpha)$  scaled by  $\alpha^{5/2}$ , as a function of  $\alpha$  on a logarithmic scale. Because  $\int \alpha^{3/2} f_r d\alpha = \int \alpha^{5/2} f_r d \ln \alpha$ , the area under the curve on the left gives the contribution of each region of  $\alpha$  to Eq. (16). The right-hand panel is the same with a logarithmic vertical scale. Notice that the non-scaling peak at  $\alpha \sim 10^{-6}$  contributes a negligible fraction of loops.

What about  $\alpha' < \Gamma G\mu$ ? In this range the coefficient of  $f_r(\alpha')$  does not decrease below  $(\Gamma G\mu)^{3/2}$  as  $\alpha'$  gets smaller. Assuming excitations on strings with wavelengths less than  $\Gamma G\mu t$  are strongly suppressed,  $f(\alpha')$  drops rapidly for  $\alpha' < \Gamma G\mu$ , so this part of the integral does not contribute. The possibility that long string excitations exist even below wavelength  $\Gamma G\mu t$  is discussed in Appendix C.

The numerator of Eq. (16) has little dependence on  $\alpha$  except for the largest loops. We can integrate the results shown in Fig. 2 to get

$$\int_0^\infty \alpha'^{3/2} f_r(\alpha') d\alpha' \approx 1.03, \quad (17)$$

which is the normalization for all loops with  $\alpha$  significantly below 0.05. Note that this result is quite different from what one would get by normalizing  $n(\alpha)$  using the flow of energy from long strings. The scaling rate of energy flow into loops in the radiation era is [48]  $2(1 - \langle v_\infty^2 \rangle) / \gamma_r^2 \approx 53$ . Energy conservation implies that this is equal to  $\int \alpha' \sqrt{p'^2 + 1} f_r d\alpha' dp'$ . If one incorrectly takes this to be  $\int \alpha' f_r d\alpha'$ , and loops to be created mainly at  $\alpha = 0.05$ , one mistakenly concludes  $\int \alpha'^{3/2} f_r(\alpha') d\alpha' \approx 53\sqrt{0.05} \approx 12$ , more than an order of magnitude too large. This error results from neglecting two important effects: (i) Even though most loops of a given size at any given time originally formed with  $\alpha \approx 0.05$ , most energy leaving the long string network goes into smaller loops (see Ref. [63]), and (ii) most of the energy leaving the network goes into loop kinetic energy, which is lost to redshifting. The latter effect is less important, since the large loops which contribute most to  $n_r(\alpha)$  are also the slowest. These effects lead to a change in constraints resulting from non-detection of gravity waves, which we discuss in Sec. III.

Using Eqs. (16) and (17), and a delta-function approximation for  $f_r(\alpha)$  peaked at the typical loop production size  $\alpha = 0.05$ , we can approximate the loop spectrum by

$$n_r(\alpha) = \frac{0.52 \Theta(0.05 - \alpha)}{(\alpha + \Gamma G\mu/2)^{5/2}}, \quad (18)$$

where  $\Theta$  is the Heaviside step function.



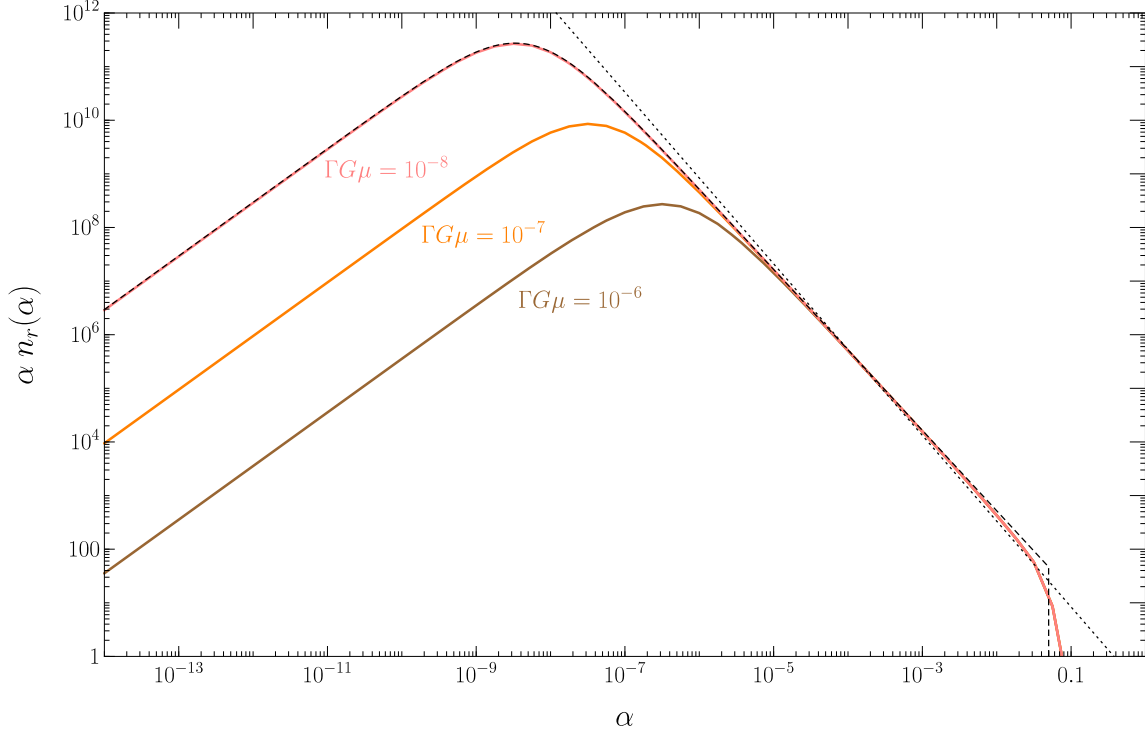


FIG. 3. The loop number density during the radiation era for various values of the evaporation rate  $\Gamma G\mu$ . Solid lines are computed from simulation data for  $f$ ; the dashed line is the analytic approximation of Eq. (18) for  $\Gamma G\mu = 10^{-8}$ . As discussed in the text, the non-scaling peak in loop production is invisible here. The dotted line represents the simulation fit in Eq. (3) of RSB [57], which agrees rather well with the results presented here.

In Fig. 3, we plot this  $n_r(\alpha)$  and the loop spectrum computed from simulation data without approximations. There are several universal features worth pointing out. For  $\alpha \gtrsim 0.05$ , there are no (non-self-intersecting) loops, since none are produced larger than this size. At smaller sizes ( $\alpha \lesssim 10^{-3}$ ), the number density grows with a slope which is universal, given by  $\alpha n(\alpha) \approx 0.6\alpha^{-3/2}$ . The peak number density per log  $\alpha$  occurs at  $\alpha = \Gamma G\mu/3$ , below which  $\alpha n(\alpha) \propto \alpha$ .

Using Eq. (18), we can find the total loop number density in scaling units,

$$n_r = \int n_r(\alpha) d\alpha \approx 0.97(\Gamma G\mu)^{-3/2}, \quad (19)$$

the average loop mass,

$$\langle \alpha \rangle_r = \frac{\int \alpha n_r(\alpha) d\alpha}{\int n_r(\alpha) d\alpha} \approx \Gamma G\mu, \quad (20)$$

and the loop matter density,

$$\langle \alpha \rangle n_r \approx 0.97(\Gamma G\mu)^{-1/2}. \quad (21)$$

The energy density in long strings [48] is about 44 in scaling units, so the energy density in

loops is larger by the factor

$$\frac{\rho_r^{\text{loops}}}{\rho_r^\infty} \approx 100 \sqrt{\left(\frac{50}{\Gamma}\right) \left(\frac{10^{-9}}{G\mu}\right)}. \quad (22)$$

Current bounds on the string tension (see Sec. III) imply the radiation era loop energy density is nearly two orders of magnitude larger than the long-string energy density, at a minimum.

Now we consider the momenta of the loops. Returning to Eq. (13), for the radiation era we find

$$n_r(\alpha, p) = \frac{\int_\alpha^\infty (\alpha' + \Gamma G\mu/2)^2 f_r(\alpha', P') d\alpha'}{2(\alpha + \Gamma G\mu/2)^3}, \quad (23)$$

with  $t' = t(\alpha + \Gamma G\mu/2)/(\alpha' + \Gamma G\mu/2)$  and thus

$$P' = \left(\frac{\alpha' + \Gamma G\mu/2}{\alpha + \Gamma G\mu/2}\right)^{1/2} p. \quad (24)$$

By writing Eq. (23) as

$$n_r(\alpha, p) = \frac{\int_\alpha^\infty (\alpha' + \Gamma G\mu/2)^{3/2} f_r(\alpha', P') \frac{\partial P'}{\partial p} d\alpha'}{2(\alpha + \Gamma G\mu/2)^{5/2}}, \quad (25)$$

we can see that integration over  $dp$  returns Eq. (16). The quantity being integrated is represented in Fig. 4.

Even though the vast majority of loops are very small ones emitted with ultra-relativistic speeds, they are suppressed by the  $\alpha'^{3/2}$  factor, so their contribution to the numerator of Eq. (23) is small. Some loops do exist with  $p \sim 2$  and  $\alpha \sim 10^{-3}$ . For these relativistic loops, the mass loss formula of Eq. (11) is not accurate. However, within a few Hubble times, before they have lost a significant fraction of their mass, these loops will be redshifted to nonrelativistic speeds. Thus the use of the nonrelativistic approximation in Eq. (11) is justified.

The number density computed using simulation data for the loop production function, and the evaporation rate  $\Gamma G\mu = 10^{-7}$  is shown in Fig. 5.

Now consider the momentum distribution of loops with a fixed  $\alpha$ . This is shown in Fig. 6 for  $\alpha = 10^{-4} \gg \Gamma G\mu$ . If  $\alpha \lesssim 10^{-3}$ , we can approximate the lower limit of integration as  $\alpha = 0$  in the numerator of Eq. (23), which thus depends on  $\alpha$  only through  $p'$ . Then the distribution for a different  $\alpha$  can be found by

$$n_r(\alpha_2, p) = \left(\frac{\alpha_1 + \Gamma G\mu/2}{\alpha_2 + \Gamma G\mu/2}\right)^3 n_r\left(\alpha_1, p \sqrt{\frac{\alpha_1 + \Gamma G\mu/2}{\alpha_2 + \Gamma G\mu/2}}\right), \quad (26)$$

so the shape of the distribution of  $n_r(\alpha, p)$  at fixed  $\alpha \lesssim 10^{-3}$  is shifted and scaled but not changed in shape under a change in  $\alpha$ .

The majority of loops (by either count or energy) at any given time have sizes  $\alpha \lesssim \Gamma G\mu$ . For such  $\alpha$ , the peak in Fig. 6 is shifted to  $p \sim \sqrt{\Gamma G\mu}$ , so this is the typical loop speed.

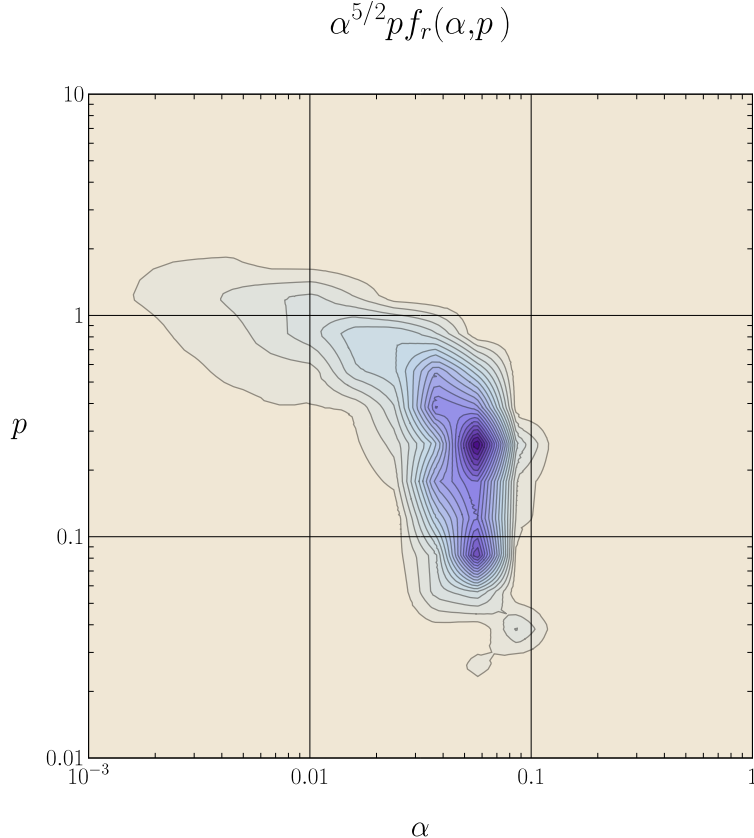


FIG. 4. Linearly spaced contours of  $\alpha^{5/2} p f_r(\alpha, p)$ , which corresponds to the quantity integrated in Eq. (25). Expansion of the universe causes any given point to flow downward and to the left at a slope of  $1/2$ .

### C. Matter era

Here we consider loops during the matter era. There are always some loops produced during the matter era, but initially they are dwarfed by relic loops from the radiation era. The exception is loops larger than  $\alpha \approx 0.05 d_h(t_{\text{eq}})/d_h(t)$ , of which none are from the radiation era.

The largest loops produced in the radiation era have size about  $0.1 t_{\text{eq}}$  and thus survive until time about  $0.1 t_{\text{eq}}/(\Gamma G\mu)$ . Thus loops remain today from the radiation era if

$$\Gamma G\mu \lesssim \frac{0.1 t_{\text{eq}}}{t_0} \approx 3.6 \times 10^{-7}. \quad (27)$$

When we use scaling units in the matter era we will always scale by the appropriate power of  $d_h \equiv 3t$ , which would be the horizon distance for a universe which had always been matter dominated, rather than taking into account the previous radiation era.

In the matter era, Eq. (15) becomes

$$n_m(t, \alpha) = \frac{\int_{\alpha}^{\alpha_{\text{eq}}} (\alpha' + \Gamma G\mu/3) f_m(\alpha') d\alpha'}{3(\alpha + \Gamma G\mu/3)^2}. \quad (28)$$

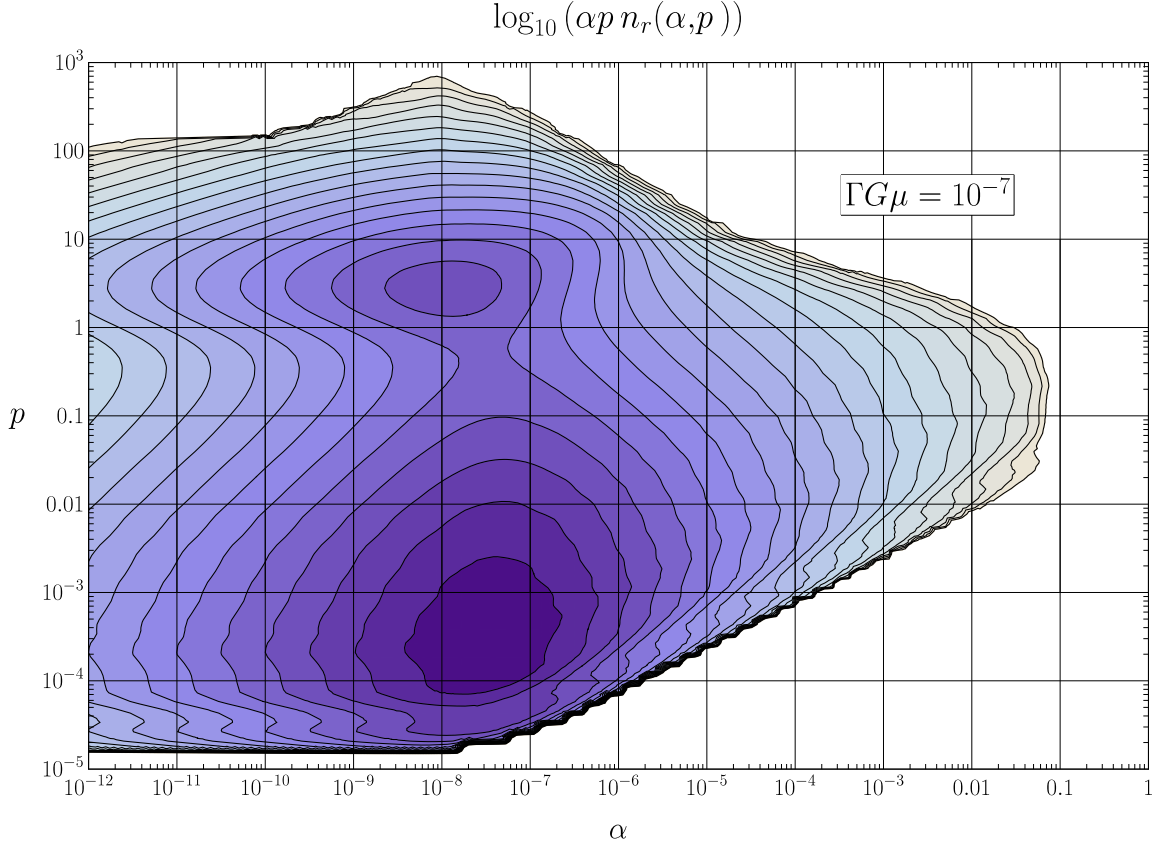


FIG. 5. The mass and momentum spectrum of loops in the radiation era, using simulation data for the loop production function and the exact flow. Contours are of  $\log_{10}(\alpha p n_r(\alpha, p))$ , with each contour representing one-half of an orders of magnitude, ranging from  $10^0$ – $10^9$ . Notice that the non-scaling peak at the top of the figure is subdominant by a few orders of magnitude; The vast majority of loops are in the scaling peak at  $\alpha \approx \Gamma G \mu / 3$ ,  $p \approx \sqrt{\Gamma G \mu}$ .

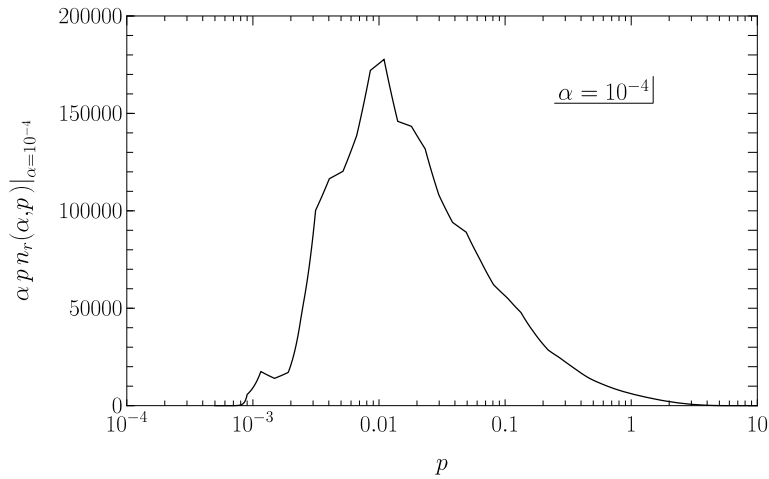


FIG. 6. The momentum distribution of loops for a slice with constant  $\alpha = 10^{-4} \gg \Gamma G \mu$  during the radiation era. For a different  $\alpha \gg \Gamma G \mu$ , the horizontal position of features in the graph is proportional to  $\alpha^{1/2}$  and the vertical position proportional to  $\alpha^{-3/2}$ .

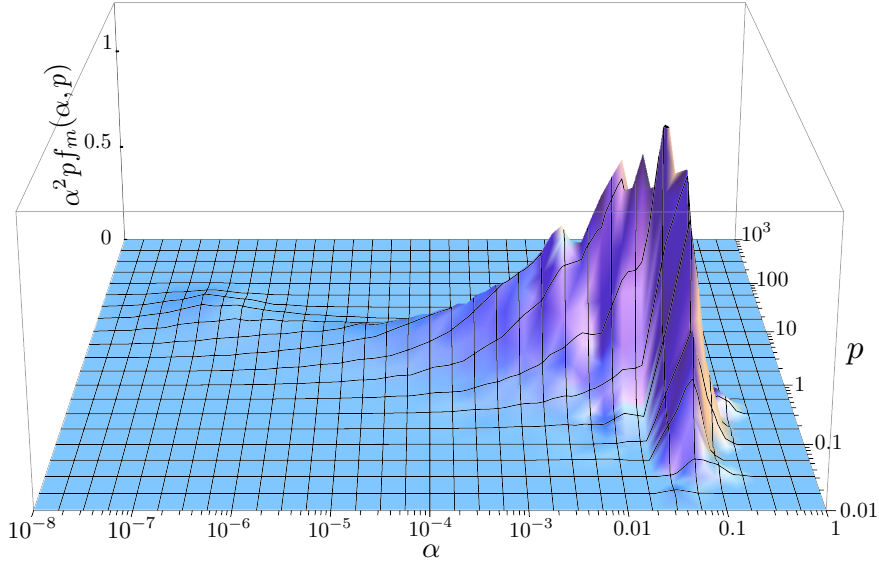


FIG. 7. The mass production function during the matter era. The non-scaling peak is almost invisible on a linear scale.

For a universe which is always been matter dominated,  $\alpha_{\text{eq}} = \infty$ , but in the real situation in there is a cutoff, because  $\alpha'$  should not be so large that the corresponding  $t' < t_{\text{eq}}$ , giving

$$\alpha_{\text{eq}} \approx \frac{t}{t_{\text{eq}}}(\alpha + \Gamma G\mu/3). \quad (29)$$

For the most part this cutoff is unimportant, since loops surviving from the radiation era will overwhelm the subpopulation affected by finite  $\alpha_{\text{eq}}$ .

The numerator in Eq. (28) is now just the total mass production function; there is no additional half power of  $\alpha'$  as there was during the radiation era. In Figs. 7 and 8, we show this quantity from 3 simulation runs of size 1000 starting at conformal time<sup>5</sup> 9 and running for time 500 for a dynamic range of 56. [48].

The simulations have reached the scaling regime, in the sense that the non-scaling peak at  $\alpha \sim 10^{-7}$  is subdominant. The behavior of tiny loops is again irrelevant for the total number of loops, thanks entirely to the large kinetic energies of small loops. As in the radiation era, if gravitational damping smooths long strings below the scale  $\Gamma G\mu t$ , then much smaller  $\alpha'$  make no contribution. The possibility of smaller smoothing scales is discussed in Appendix C.

In Eq. (28), the smaller power of  $\alpha'$  multiplying the loop production function means that loop production effectively happens over a broader hierarchy of scales, as compared with the radiation era. Hence, the number density  $n(\alpha)$ , which is the integral of this broad production, will approach the universal power law  $\alpha^{-1}$  much more slowly, having a steeper slope at larger  $\alpha$ . This may explain why the numerical fit of RSB is steeper than the universal slope, since the fit was performed at large  $\alpha$ .

<sup>5</sup> In previous work [48], we used starting time 4.5 in the matter era. The present choice of 9.0 makes the large-loop part of the loop production function closer to its scaling value at early times.

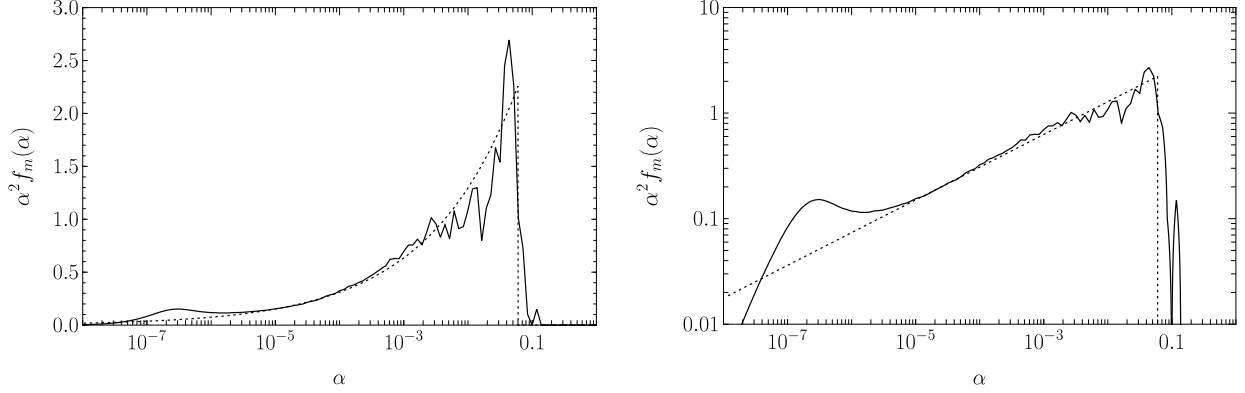


FIG. 8. The loop production rate  $f(\alpha)$  scaled by  $\alpha^2$ . The non-scaling peak represents a subdominant contribution to the total number of loops, although it may contribute significantly to the small loop sub-population. The dotted line shows the approximation of Eq. (30). Note that the non-scaling peak would be more prominent in these graphs if we were to use the scaling energy instead of the rest mass of the loops. See the corresponding figures in [48]. This is due to the fact that most of the energy of the small loop population is in kinetic energy, not rest mass.

An analytic approximation for the matter era loop production function is

$$f_m(\alpha) \approx \frac{5.34}{\alpha^{1.69}} \Theta(0.06 - \alpha) \quad (30)$$

shown in Fig. 8. Neglecting any possible contribution from  $\alpha < \Gamma G\mu$ , Eq. (30) results in the analytic approximation for the scaling loop spectrum,

$$n_m(\alpha) \approx \frac{2.4 - 5.7\alpha^{0.31}}{(\alpha + \Gamma G\mu/3)^2}, \quad (31)$$

and its integral

$$n_m \approx 7.2(\Gamma G\mu)^{-1}. \quad (32)$$

We illustrate  $n_m(\alpha)$  in Fig. 9, using simulation data and the non-relativistic loop evaporation rate. Including the transient effect of  $\alpha_{\text{eq}}$  gives

$$n_m(t, \alpha) \approx \frac{(2.4 - 5.7\alpha^{0.31}) \Theta(0.06 - \alpha) - (2.4 - 5.7\alpha_{\text{eq}}^{0.31}) \Theta(0.06 - \alpha_{\text{eq}})}{(\alpha + \Gamma G\mu/3)^2}. \quad (33)$$

Now we consider momenta in the matter era. Equation (13) gives

$$n_m(t, \alpha, p) = \frac{\int_{\alpha}^{\alpha_{\text{eq}}} (\alpha' + \Gamma G\mu/3)^{5/3} f_r(\alpha', P') d\alpha'}{3(\alpha + \Gamma G\mu/3)^{8/3}}, \quad (34)$$

with  $t' = t(\alpha + \Gamma G\mu/3)/(\alpha' + \Gamma G\mu/3)$  and thus

$$P' = \left( \frac{\alpha' + \Gamma G\mu/3}{\alpha + \Gamma G\mu/3} \right)^{2/3} p. \quad (35)$$

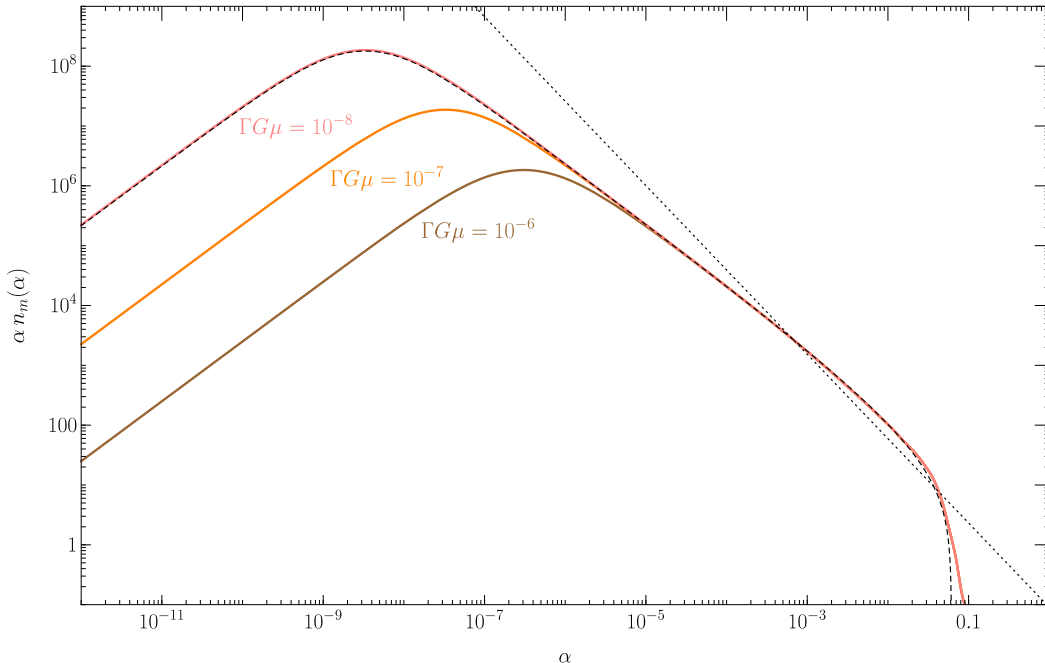


FIG. 9. The loop number density during the matter era for various values of the evaporation rate  $\Gamma G\mu$ . Solid lines use pure simulation data for the loop production function and the non-relativistic loop evaporation rate. The dashed line is the analytic approximation of Eq. (31) for  $\Gamma G\mu = 10^{-8}$ . The dotted line represents the fit (roughly for  $10^{-3} \lesssim \alpha \lesssim 10^{-1}$ ) in Eq. (3) of RSB [57]. Although this fit cannot be extrapolated to small  $\alpha$ , the data appear consistent with our results.

By writing this as

$$n_m(t, \alpha, p) = \frac{\int_{\alpha}^{\alpha_{\text{eq}}} (\alpha' + \Gamma G\mu/3) f_r(\alpha', P') \frac{\partial P'}{\partial p} d\alpha'}{3(\alpha + \Gamma G\mu/3)^2}, \quad (36)$$

we can see that integration over  $dp$  returns Eq. (28). The object being integrated is represented in Fig. 10. In Fig. 11, we show the distribution of loops in a matter-dominated universe, including relativistic effects on loop evaporation.

In this case, there is a substantial tail extending to high boost. When we use the nonrelativistic formula for mass lost to gravity waves, Eq. (11), we overestimate the change by a factor  $\gamma$ . This overestimate occurs until the loop momentum per unit mass falls from  $p$  to of order unity. If the loop is created at time  $t_i$ , this happens at  $t_{\text{nr}}$  where  $a(t_{\text{nr}})/a(t_i) = p$ , or  $t_{\text{nr}} = p^{3/2}t_i$ . For large  $p$ , the overestimate of the total emitted mass is  $\Gamma G\mu^2 t_{\text{nr}} = \Gamma G\mu^2 p^{3/2}t_i$ . This is of little consequence providing it is much less than the the original loop mass  $\alpha d_h\mu = 3\alpha t_i\mu$ . Thus we consider what fraction of the integral in numerator of Eq. (28) is made up of high-momentum loops with

$$\Gamma G\mu p^{3/2} > 3\alpha. \quad (37)$$

Even for very heavy strings with  $\Gamma G\mu = 10^{-5}$  this fraction only is about 11%, and for  $\Gamma G\mu = 10^{-7}$  it is about 5%, so there is some error from this effect, but not a very large one.

The distribution of velocities for loops with a fixed  $\alpha = 10^{-6}$ , assuming this is still greater than  $\Gamma G\mu$ , is shown in Fig. 12. Note that this is about the smallest  $\alpha$  which today describes

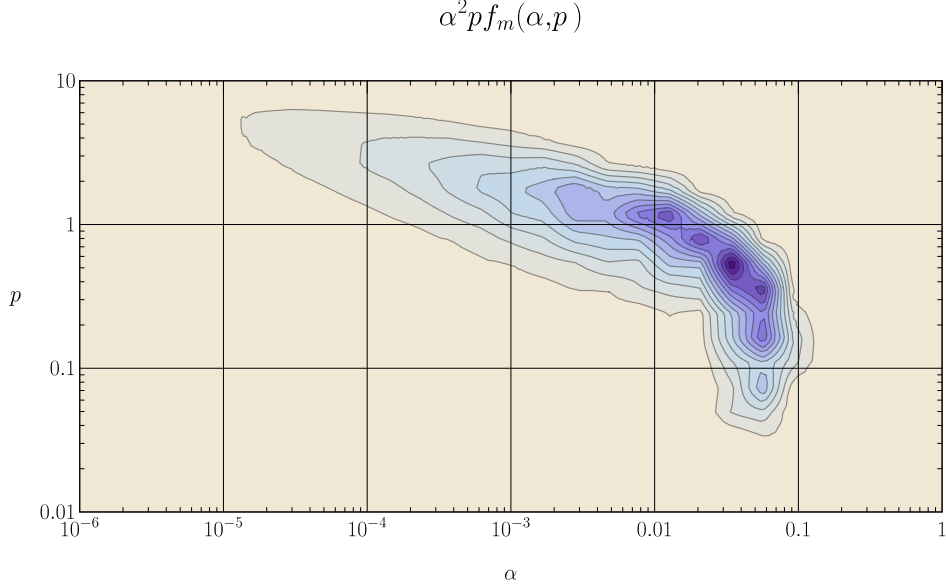


FIG. 10. A contour plot of the mass production function during the matter era. This is the quantity relevant for determining the matter era loop number density. Expansion of the universe causes any given point to flow downward and to the left at a slope of  $2/3$ . Contours are of  $\alpha^2 p f_m(\alpha, p)$ , spaced linearly from 0.1–1.3.

loops formed in the matter era. Smaller loops would be relics from the radiation era, which we discuss in the next subsection.

The velocity of a typical loop is around  $10(\Gamma G\mu)^{2/3}$ , but the distribution is quite broad.

#### D. Loops surviving from the radiation era

Most loops in existence during the matter era were produced during the radiation era. A loop of size  $\alpha$  at time  $t$  in the matter era has mass  $m = 3\mu\alpha t$  and thus had mass  $M_{\text{eq}} = 3\mu\alpha t + \Gamma G\mu^2(t - t_{\text{eq}})$  at  $t_{\text{eq}}$ . Thus, at the end of the radiation era with  $d_h = 2t_{\text{eq}}$ , this loop had

$$\alpha_{\text{eq}} = \frac{1}{2} \left[ (3\alpha + \Gamma G\mu) \frac{t}{t_{\text{eq}}} - \Gamma G\mu \right] \approx \frac{(3\alpha + \Gamma G\mu)t}{2t_{\text{eq}}}. \quad (38)$$

In range of sizes  $d\alpha$  at  $t_{\text{eq}}$  there were  $n_r(\alpha)d\alpha$  loops in a horizon volume,  $(2t_{\text{eq}})^3$ , and thus per comoving volume there were  $n_r(\alpha)d\alpha(a_{\text{eq}}^3/(2t_{\text{eq}})^3)$ . These loops become the loops in the same comoving volume at a later time  $t$ , so

$$n_r(t > t_{\text{eq}}, \alpha) = n_r(\alpha_{\text{eq}}) \frac{a_{\text{eq}}^3}{a^3(t)} \frac{(3t)^3}{(2t_{\text{eq}})^3} \frac{\partial \alpha_{\text{eq}}}{\partial \alpha} = \frac{81t^2}{16t_{\text{eq}}^2} n_r(\alpha_{\text{eq}}), \quad (39)$$

with  $\alpha_{\text{eq}}$  given by Eq. (38). This is time-dependent, since it is not a scaling population. It should be pointed out that the apparent discontinuity in  $n_r(t, \alpha)$  at  $t_{\text{eq}}$  is only due to the discontinuity in our choice of the “horizon distance”  $d_h = 2t \rightarrow 3t$  at  $t = t_{\text{eq}}$ . The loop number density is, of course, continuous at  $t = t_{\text{eq}}$ .



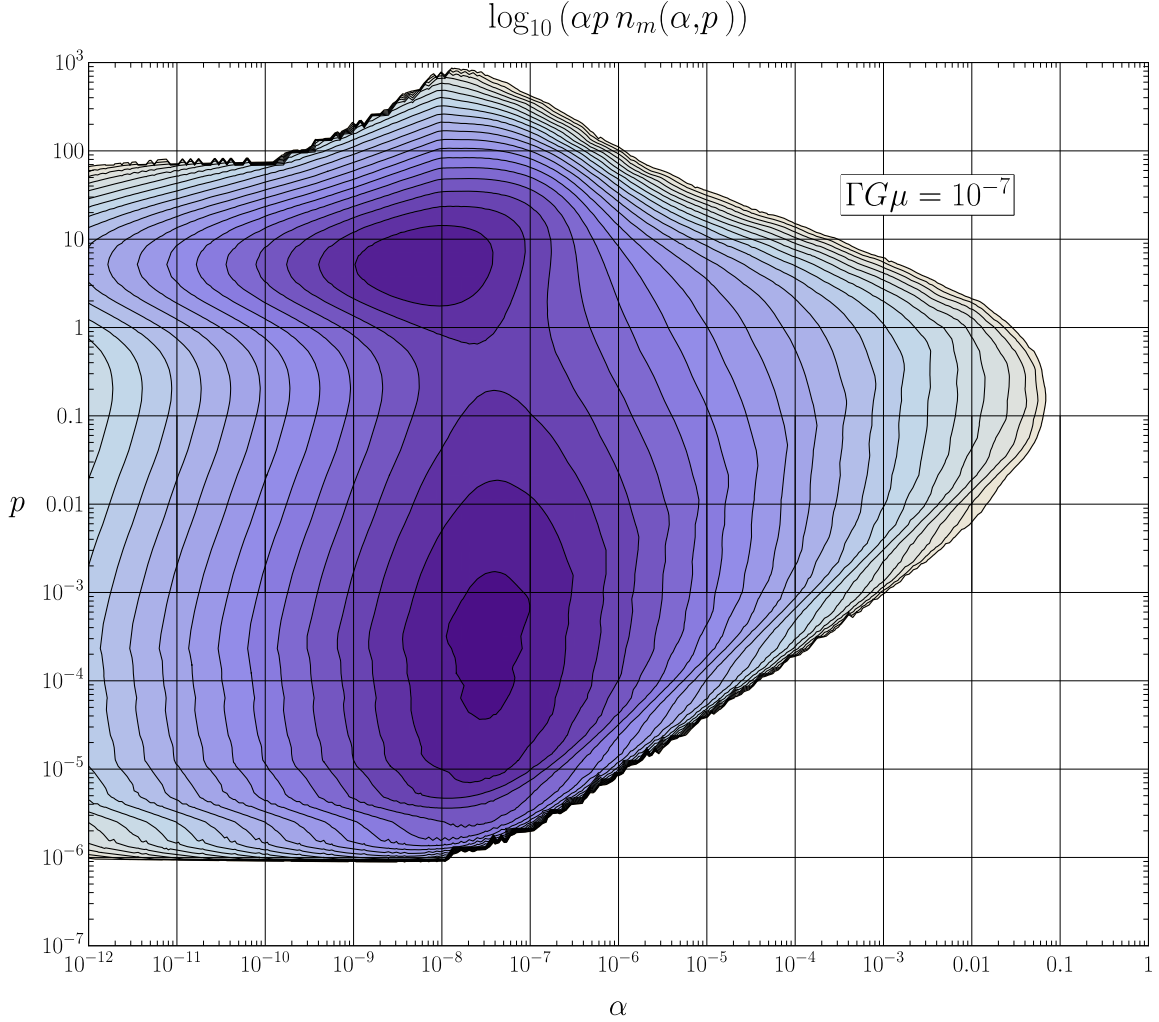


FIG. 11. The mass and momentum spectrum of loops in a matter dominated universe, using simulation data for the loop production function and the exact flow. Contours are of  $\log_{10}(\alpha p n_r(\alpha, p))$ , with each contour representing one-third of an order of magnitude, ranging from  $10^0$ – $10^{19/3}$ . Notice that the non-scaling peak at the top of the figure is subdominant by an order of magnitude; The majority of loops are in the scaling peak at  $\alpha \approx \Gamma G\mu/3, p \approx 10 (\Gamma G\mu)^{2/3}$ .

Plugging in the analytic approximation from Eq. (18), we find

$$n_r(t > t_{\text{eq}}, \alpha) \approx 2.6 \frac{t^2}{t_{\text{eq}}^2} \frac{\Theta(0.05 - \alpha_{\text{eq}})}{(\alpha_{\text{eq}} + \Gamma G\mu/2)^{5/2}} \quad (40)$$

$$\approx 0.94 \left( \frac{t_{\text{eq}}}{t} \right)^{1/2} \frac{\Theta(0.03(t_{\text{eq}}/t) - \alpha - \Gamma G\mu/3)}{(\alpha + \Gamma G\mu/3)^{5/2}}. \quad (41)$$

The most important loops are those with  $\alpha \sim \Gamma G\mu$ . Ignoring numerical factors, if  $\Gamma G\mu \gtrsim t_{\text{eq}}/t$  then these loops were formed in the matter era, and if  $\Gamma G\mu \lesssim t_{\text{eq}}/t$  they were formed in the radiation era. The latter is the case for all realistic values of string tension. Equation (40) has an extra half power of  $\alpha + \Gamma G\mu/3$  in the denominator as compared to Eq. (31). For  $\alpha \sim \Gamma G\mu \sim t_{\text{eq}}/t$  this is canceled by the prefactor, but for smaller  $\Gamma G\mu$  the

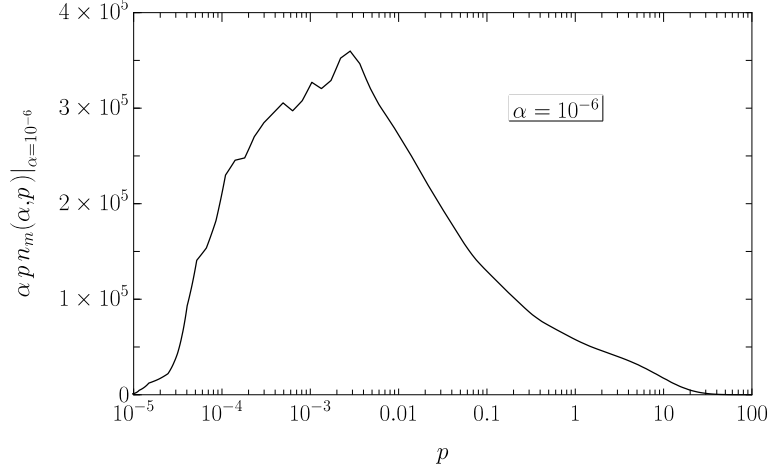


FIG. 12. The momentum distribution of loops with  $\alpha = 10^{-6} \gg \Gamma G\mu$  in a matter dominated universe for a slice at constant  $\alpha$ . For a different  $\alpha \gg \Gamma G\mu$ , the horizontal position of features in the graph is proportional to  $\alpha^{2/3}$  and the vertical position proportional to  $\alpha^{-2}$ .

number of loops is enhanced by  $\sqrt{t_{\text{eq}}/(\Gamma G\mu t)}$  over what it would be in a purely matter universe.

### III. STOCHASTIC GRAVITATIONAL WAVES AND A BOUND ON $G\mu$

The contribution of cosmic string loops to the stochastic background of gravitational waves was recognized as one of the most significant observational signatures of a network of strings, and over the years it has been calculated by several groups with various different assumptions [1–14].

Having obtained a robust description of the distribution of loops from our simulations we can now use it to update the calculation of the spectrum of energy in gravitational waves,  $\Omega_{\text{gw}}(\ln f)$ , with  $\Omega_{\text{gw}}(\ln f)d\ln f$  being the fraction of the critical density in gravitational waves whose frequencies lie between  $f$  and  $f + fd\ln f$ . We define the gravitational wave energy per (physical) volume per unit frequency  $\rho_{\text{gw}}(t, f)$ , and then divide by the critical energy density to obtain

$$\Omega_{\text{gw}}(\ln f) = \frac{8\pi G}{3H_0^2} f \rho_{\text{gw}}(t_0, f). \quad (42)$$

We let  $\mathcal{P}_{\text{gw}}(t, f)df$  be the power per physical volume flowing into gravitational waves of frequencies between  $f$  and  $f + df$ . Then  $\rho_{\text{gw}}$  is just the time integral of  $\mathcal{P}_{\text{gw}}$ , taking into account the  $a^{-4}$  scaling of radiation energy densities and the redshifting of frequency,

$$\rho_{\text{gw}}(t, f) = \int_0^t dt' \frac{a^4(t')}{a^4(t)} \mathcal{P}_{\text{gw}}(t', F') \frac{\partial F'}{\partial f} = \int_0^t dt' \frac{a^3(t')}{a^3(t)} \mathcal{P}_{\text{gw}}\left(t', \frac{a(t)}{a(t')} f\right), \quad (43)$$

where  $F' = \frac{a}{a'} f$ .

The power per volume  $\mathcal{P}_{\text{gw}}$  is given by the comoving number density of loops  $n(t, m)$ , and the power  $P$  radiated by each loop,

$$\mathcal{P}_{\text{gw}}(t, f) = \int dm \frac{n(t, m)}{a^3(t)} P(m, f). \quad (44)$$

Assuming most loops develop and maintain at least one cusp per oscillation for much of their evolution, the power radiated by a slowly moving loop of mass  $m$  is approximately

$$P(m, f) = \frac{\Gamma G \mu^2}{\zeta(\frac{4}{3}, j_*)} \sum_{j=1}^{j_*} j^{-4/3} \delta\left(f - j \frac{2\mu}{m}\right), \quad (45)$$

where the maximum allowed harmonic is  $j_*$  (which we will assume to be infinite),  $\zeta(\frac{4}{3}, j_*) = \sum_{j=1}^{j_*} j^{-4/3} \approx 3.60$ , and we have used the fact that the the period of the loop is  $\frac{m}{2\mu}$ . The spectral index  $q = 4/3$  represents the high frequency behavior of cusp emission.

Putting this together yields

$$\rho_{\text{gw}}(t_0, f) = \frac{\Gamma G \mu^2}{\zeta(\frac{4}{3}, j_*)} \sum_{j=1}^{j_*} j^{-4/3} \int_0^{t_0} dt \int dm \frac{n(t, m)}{a^3(t_0)} \delta\left(\frac{a(t_0)}{a(t)} f - j \frac{2\mu}{m}\right), \quad (46)$$

and so the fractional spectrum today is

$$\Omega_{\text{gw}}(\ln f) = \frac{8\pi \Gamma G^2 \mu^2 f}{3H_0^2 \zeta(\frac{4}{3}, j_*)} \sum_{j=1}^{j_*} j^{-4/3} \int_0^{t_0} dt \int dm \frac{n(t, m)}{a_0^3} \delta\left(\frac{a_0}{a(t)} f - j \frac{2\mu}{m}\right), \quad (47)$$

$$= \frac{8\pi \Gamma G^2 \mu^2 f}{3H_0^2 \zeta(\frac{4}{3}, j_*)} \sum_{j=1}^{j_*} j^{-4/3} \int_0^\infty \frac{dz}{H(z)(1+z)} \int dm \frac{n(t(z), m)}{a_0^3} \delta\left((1+z)f - j \frac{2\mu}{m}\right), \quad (48)$$

$$= \frac{8\pi \Gamma G^2 \mu^2}{3H_0^2 \zeta(\frac{4}{3}, j_*)} \sum_{j=1}^{j_*} j^{-4/3} \int_0^\infty \frac{dz}{H(z)(1+z)^3} \frac{n(t(z), \frac{2\mu j}{(1+z)f})}{a_0^3} \frac{2\mu j}{f}, \quad (49)$$

where we have used the fact that  $dt = -dz/[H(z)(1+z)]$ . For  $z \gtrsim 1$  the functions  $H(z)$  and  $t(z)$  are well approximated by the matter-plus-radiation solution

$$H_{m+r}(z) = H_0 \sqrt{\Omega_{m,0} (1+z)^3 \left(1 + \frac{1+z}{1+z_{\text{eq}}}\right)} \quad (50)$$

$$t_{m+r}(z) = \frac{2}{3H_0 \sqrt{\Omega_{m,0} (1+z_{\text{eq}})^{3/2}}} \left(2 + \sqrt{1 + \frac{1+z_{\text{eq}}}{1+z} \left(\frac{1+z_{\text{eq}}}{1+z} - 2\right)}\right). \quad (51)$$

Although we neglect the details of loop production in a matter-plus-radiation universe, the radiation era comoving loop number density is not significantly affected by the smooth transition to matter domination, certainly for the small ( $\alpha \sim \Gamma G \mu$ ) loops which are important. Thus for  $t \leq t_{\text{eq}} = t_{m+r}(z_{\text{eq}})$ , the comoving loop number density is well approximated by the pure radiation value of Eq. (18), converted to comoving units using Eq. (4),

$$n_r(t(z), m) \approx \frac{a_r^3}{\mu d_{h,r}^4} n_r(\alpha_r), \quad (52)$$

where  $\alpha_r = \frac{m}{\mu d_{h,r}}$ ,  $d_{h,r} = 2t(z)$ , and  $a_r = \sqrt{\frac{t(z)}{t_{\text{eq}}}} \frac{a_0}{1+z_{\text{eq}}} \frac{2}{\sqrt{3+3/\sqrt{2}}}$ . The numerical factors in  $a_r$  are chosen such that  $a_r \rightarrow a_0/(1+z)$  for  $z \gg z_{\text{eq}}$ .

For  $t > t_{\text{eq}}$ , the most numerous loops are those which survive from the radiation era,

$$n_{r \rightarrow m}(t(z), m) = n_r(t_{\text{eq}}, m + \Gamma G \mu^2 [t(z) - t_{\text{eq}}]). \quad (53)$$

The loops produced during the matter era are given by Eq. (33) and

$$n_m(t(z), m) = \frac{a_m^3}{\mu d_{h,m}^4} n_m(t(z), \alpha_m), \quad (54)$$

where  $\alpha_m = \frac{m}{\mu d_{h,m}}$ ,  $d_{h,m} = 3t(z)$ , and  $a_m = \left(\frac{t(z)}{t_{\text{eq}}}\right)^{2/3} \frac{a_0}{1+z_{\text{eq}}} (2 - \sqrt{2})^{2/3}$ . The numerical factors in  $a_m$  are chosen such that  $a_m \rightarrow a_0/(1+z)$  for  $z \ll z_{\text{eq}}$ .

Dark energy becomes important for  $z \lesssim 1$ . Although the additional dilution is already taken into account since we use comoving number densities, we should now compute cosmic time  $t(z)$  using the  $\Lambda$ -plus-matter solution

$$H_{\Lambda+m}(z) = H_0 \sqrt{\Omega_\Lambda + \Omega_{m,0}(1+z)^3}, \quad (55)$$

$$t_{\Lambda+m}(z) = \frac{2 \tanh^{-1} (H_0 \sqrt{\Omega_\Lambda} / H_{\Lambda+m}(z))}{3H_0 \sqrt{\Omega_\Lambda}} + C_9, \quad (56)$$

where  $\Omega_\Lambda = 1 - \Omega_{m,0}$ , and  $C_9$  is chosen to make  $t_{\Lambda+m}(z) = t_{m+r}(z)$  at some matter dominated splicing redshift, say  $z = 9$ .

By using the matter-era simulated  $n_m(\alpha)$ , and just plugging  $t(z) \rightarrow t_{\Lambda+m}(z)$  in Eq. (54) and below, we are making the assumption that the comoving loop production function is unaffected by dark energy. This is certainly true for all but the largest loops, since production of small loops is always negligible.

Put another way, the vast majority of loops today were produced at  $z \gg 1$ , when matter-era simulation data can be trusted. The Boltzmann equation, Eq. (A14), is just

$$n(t, m) = n(t_i, m + \Gamma G \mu^2 (t - t_i)) + \int_{t_i}^t f(t', m + \Gamma G \mu^2 (t - t')) dt', \quad (57)$$

which says that for any loop sizes whose recent production rate is negligible (i.e.,  $f(t', M') = 0$ ), we simply take the previously understood comoving number density at time  $t_i$ , and age it by  $t - t_i$ . It is irrelevant whether we use  $f_m$  or the true  $f_{\Lambda+m}$ , since they both vanish for the vast majority of loops which exist for  $0 \leq z \lesssim 1$ . Hence using  $n_m(t, m)$  today is justified provided we don't care about loops larger than about 2% of the size of the observable universe. Note that this is only true in comoving units, since scaling units assume the wrong horizon size, and physical units neglect the extra dilution due to dark energy. We can always convert to physical units using scale factor  $a_0/(1+z)$ , rather than  $a_m(t_{\Lambda+m}(z))$ .

Putting the comoving number densities, Eqs. (52–54), into Eq. (49), and using the analytic approximations for the Hubble rate and proper time, Eqs. (50–51) and Eqs. (55–56) for redshifts above and below  $z = 9$ , respectively, we numerically compute the stochastic gravitational wave background for various values of  $G\mu$ , assuming  $\Gamma = 50$ , shown in Fig. 13.

The high frequency behavior is independent of the spectral index  $q = 4/3$ , and can be written analytically for  $f \gg (1 + z_{\text{eq}})/(\Gamma G \mu t_{\text{eq}})$  as

$$\Omega_{\text{gw}}(\ln f) \rightarrow \frac{8\pi \Gamma G^2 \mu^2 \Omega_{m,0}}{3(1 + z_{\text{eq}})} \int_0^1 n_r(\alpha) d\alpha, \quad (58)$$

$$\approx 8.14 \frac{\Omega_{m,0}}{1 + z_{\text{eq}}} \sqrt{\frac{G\mu}{\Gamma}}, \quad (59)$$

$$\approx 7.7 \times 10^{-4} \sqrt{\frac{G\mu}{\Gamma}}, \quad (60)$$

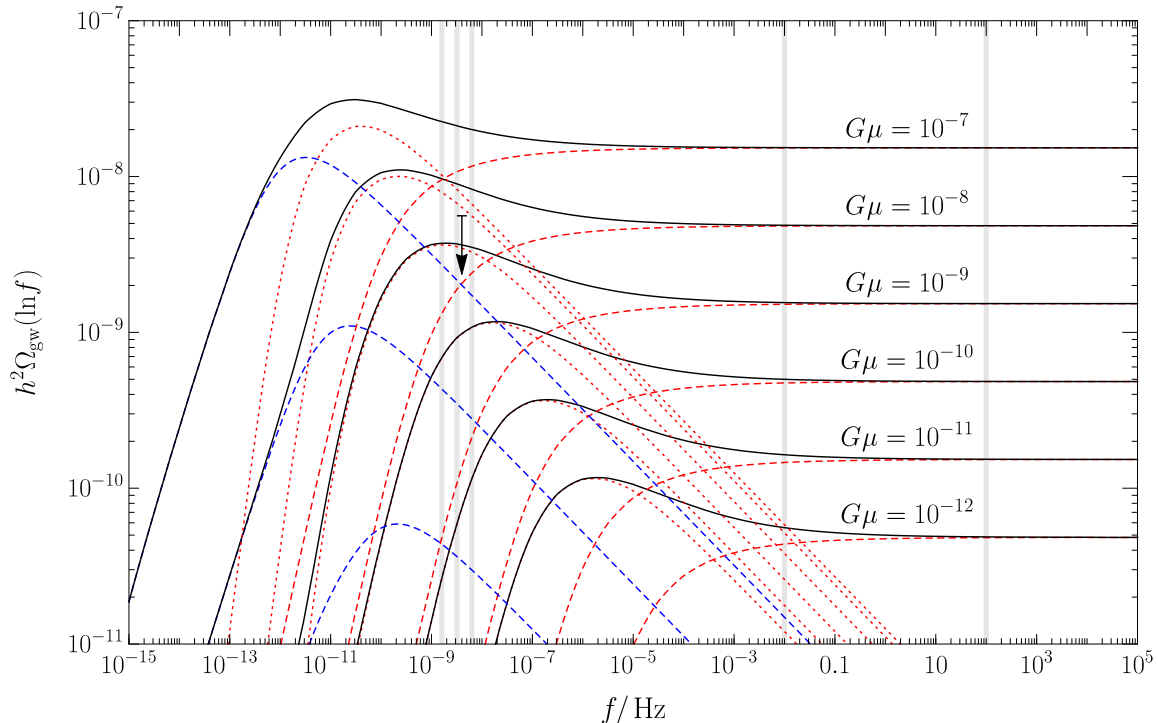


FIG. 13. The normalized spectrum of gravitational waves for various values of string tension. The red dashed lines show the contribution from loops radiating during the radiation era, the red dotted lines represent the contribution from loops produced during the radiation era, but radiating during the matter era, and the blue dashed lines represent loops produced during the matter era. In light gray from left to right, the 20-, 10-, and 5-year PTA, eLISA [12, 65] and LIGO [66] peak sensitivity frequencies are shown.

where we are using the best-fit cosmological parameters from Planck + WMAP polarization [64],  $z_{\text{eq}} = 3403$ ,  $\Omega_{m,0} = 0.3183$ , and  $H_0 = 2.171 \times 10^{-18} \text{ Hz}$ , i.e.,  $h = 0.6704$ .

In Fig. 14 we graph the string tension  $G\mu$  vs. the normalized power in gravitational waves for five characteristic detector frequencies. Currently, the most stringent limits on  $G\mu$  come from pulsar timing arrays (e.g. [67], [68]). Following the analysis of Ref. [10] on the data of Ref. [67], we use the 95% confidence limit  $h^2\Omega_{\text{gw}}(f = 4.0 \times 10^{-9} \text{ Hz}) \leq 5.6 \times 10^{-9}$ , which using our loop distribution provides the bound on tension

$$G\mu \leq 2.8 \times 10^{-9}, \quad (61)$$

as shown in Fig. 14. Notice that this bound is consistent with the range of tensions expected from cosmic superstrings, which are produced after brane inflation [69]. This bound should not be taken as definitive, since we have neglected several effects, including changes in the number of relativistic degrees of freedom at early times, the actual spectrum of gravitational emission from realistic loops, the possibility that some energy is in rare bursts that we would not have observed [20], and the possible fragmentation of loops after significant gravitational backreaction. We intend to do a more careful analysis of the gravitational wave signature of loops including all these effects.

We can compare this bound with the results of Ref. [10], which found  $G\mu < 8.8 \times 10^{-11}$  for the case of all loops being produced with scaling energy  $x = 0.05$ . We believe the order

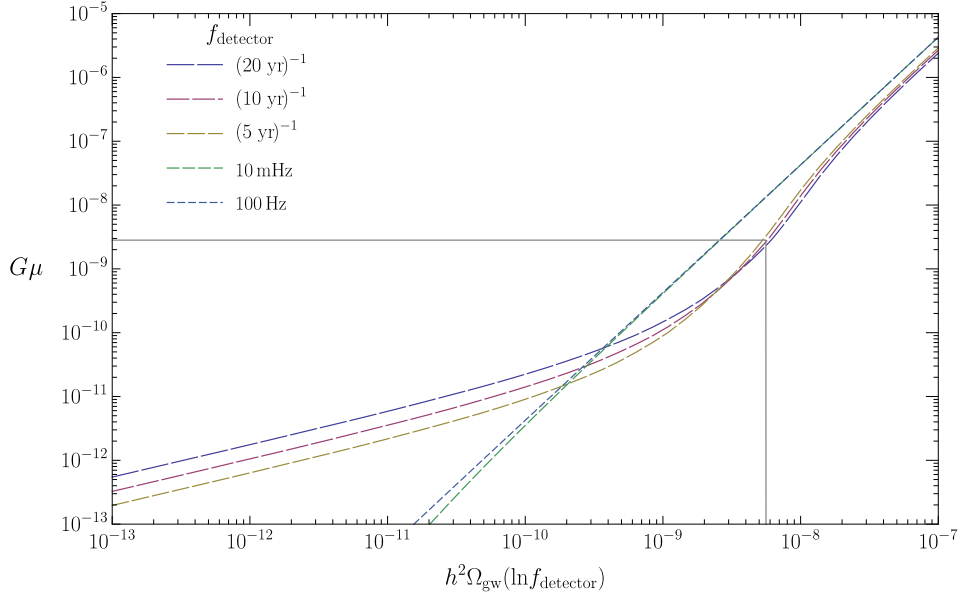


FIG. 14. Constraints on  $G\mu$  for five detector peak sensitivity frequencies. The horizontal axis is the upper bound on  $h^2\Omega_{\text{gw}}$  provided by a particular experiment, and the vertical axis represents the corresponding upper bound on the cosmic string tension. The five frequencies plotted are shown in the legend, with PTA detector frequencies given by the inverse of the duration of the experiment. The gray solid lines indicate the bound of Eq. (61).

of magnitude discrepancy is primarily due to the fact that only about 10% of power actually flows into the largest loops, as discussed below Eq. (17). A precise comparison is difficult, since both our loop sizes and velocities differ from models they considered.

#### IV. CONCLUSIONS

By extrapolation from loop production found in simulations, we give the distribution of loops to be found in the universe at any given time. While some uncertainties remain in the late-time behavior of the loop production function, these make no significant contribution to the loop number density. The numerical value for the loop number density arising from simulations over the past decade is now rather well agreed upon, with numerical coefficients roughly of order unity [48, 57–59].

In the radiation era, in scaling units we find to good approximation

$$n_r(\alpha) \approx \frac{0.52}{(\alpha + \Gamma G\mu/2)^{5/2}}, \quad (62)$$

up to a cutoff at  $\alpha \approx 0.05$ . In physical units, this gives

$$\frac{n_r(t, l)}{a^3(t)} \approx \frac{0.18}{t^{3/2}(l + \Gamma G\mu t)^{5/2}}, \quad (63)$$

up to a cutoff at  $l \approx 0.1t$ . While the functional form agrees with Eq. (10.1.12) of Ref. [70], it differs by a significant numerical factor.

In the matter era, we have

$$n_m(\alpha) \approx \frac{2.4 - 5.7\alpha^{0.31}}{(\alpha + \Gamma G\mu/3)^2} \quad (64)$$

for  $\alpha < 0.06$ , or in physical units

$$\frac{n_m(t, l)}{a^3(t)} \approx \frac{0.27 - 0.45(l/t)^{0.31}}{t^2(l + \Gamma G\mu t)^2}, \quad (65)$$

for  $l < 0.18t$ . (We ignore the small loop cutoff of Eq. (29), since radiation era loops dominate regardless.) For  $l \ll t$ , the second term in the numerator can be ignored, and then Eq. (65) agrees with Eq. (10.1.17) of Ref. [70] except for numerical factors.

Most importantly in the matter era, there will be loops remaining from the radiation era, given by

$$n_r(t > t_{\text{eq}}, \alpha) \approx \frac{0.94t^{1/2}}{t_{\text{eq}}^{1/2}(\alpha + \Gamma G\mu/3)^{5/2}} \quad (66)$$

for  $\alpha < 0.03(t_{\text{eq}}/t) - \Gamma G\mu/3$ , or

$$\frac{n_r(t > t_{\text{eq}}, l)}{a^3(t)} \approx \frac{0.18t_{\text{eq}}^{1/2}}{t^2(l + \Gamma G\mu t)^{5/2}} \quad (67)$$

for  $l < 0.09t_{\text{eq}} - \Gamma G\mu t$ . This agrees with Eq. (10.1.20) of Ref. [70], except for a significant numerical factor, and the effects of evaporation.

The above calculations are for a pure matter era (with a sudden transition from a pure radiation era at  $t_{\text{eq}}$ ). Embedding these results into a realistic cosmology is done in Sec. III. The calculation is simpler if we are only interested in the loop number density today, which we can compute in a way which depends only on the present content and age of the universe, as follows.

First consider relics from the radiation era. Let  $t_r$  and  $z_r$  be some time and corresponding redshift in the radiation era. The loop density at  $t_r$  is given by Eq. (63). The density of the same loops today is just given by dilution,

$$\frac{n_r(t_0, l)}{a_0^3} = \frac{0.18}{(1 + z_r)^3 t_r^{3/2} (l + \Gamma G\mu t_0)^{5/2}} \quad (68)$$

for  $l < 0.09t_{\text{eq}} - \Gamma G\mu t_0$ . In the radiation era, we have

$$\frac{1}{4t_r^2} = H^2(t_r) = H_0^2 \Omega_{r,0} (1 + z_r)^4 \quad (69)$$

and thus

$$\frac{n_r(t_0, l)}{a_0^3} = \frac{0.51(H_0^2 \Omega_{r,0})^{3/4}}{(l + \Gamma G\mu t_0)^{5/2}} \quad (70)$$

Here  $\Omega_r$  refers to the radiation density that we would have today with the present CMB temperature and neutrinos being massless, i.e., the one that we could extrapolate backward into the radiation era when neutrino masses did not matter.

Since

$$H_0^2 \Omega_{r,0} = \frac{8\pi G}{3} \rho_r(T_0), \quad (71)$$

$n_r(t_0, l)/a_0^3$  can be computed from the present-day CMB temperature  $T_0$  and the current age of the universe,  $t_0$ .

We can make a similar calculation for loops produced in the matter era. Let  $t_m$  and  $z_m$  be some time and redshift when the universe was matter-dominated, before dark energy became important. Use Eq. (65) at  $t_m$ , and then advance to the present. In the matter era, we have

$$\frac{4}{9t_m^2} = H^2(t_m) = H_0^2 \Omega_{m,0} (1 + z_m)^3 \quad (72)$$

and thus

$$\frac{n_m(t_0, l)}{a_0^3} \approx \frac{0.61 - 1.0(l/t_0)^{0.31}}{(l + \Gamma G \mu t_0)^2} H_0^2 \Omega_{m,0}, \quad (73)$$

The presence of  $t_0$  in the numerator of Eq. (73) is correct only in the approximation that loop production continues unchanged during dark energy domination. The opposite case, in which loop production stops entirely, can be approximated by writing  $t_m$  instead of  $t_0$  in the numerator of Eq. (73), and setting  $t_m$  to the start of the dark energy era. But the effect is small and applies only to fairly large loops. The density of the very largest loops could be determined only by simulations of the matter to dark energy transition, but such loops are so rare as to be of very little observational interest.

## ACKNOWLEDGMENTS

We thank Joe Polchinski, Christophe Ringeval, Xavier Siemens, Vitaly Vanchurin and Alex Vilenkin for helpful discussions. This work was supported in part by the National Science Foundation under grants 0855447, 0903889, 1213888, and 1213930 and by the Spanish Ministry of Science and Technology under the FPA2009-10612 and FPA2012-34456 grants.

## Appendix A: Differential forms

### 1. Introduction

Quantities such as the density of loops are more elegantly described using differential forms. Thus instead of taking  $n(\alpha)$  as our fundamental quantity, we take the 1-form  $n(\alpha)d\alpha$ . The definition of this differential form is the object which, when integrated over a range of  $\alpha$ , gives the number of loops whose sizes lie in that range. This avoids some awkwardness in defining the function  $n(\alpha)$ , and makes the transformation between physical and scaling coordinates clear.

Since a differential form returns physical, coordinate-independent values upon integration, it is the area under the curve (or surface) that we use to represent it, rather than the height of the curve. In this regard it is very much like a probability density function. For example, in a graph of  $n(\alpha)d\alpha$  with  $\alpha$  on a linear scale, the area under the curve  $n(\alpha)$  faithfully



represents the integral  $\int n(\alpha)d\alpha$ . But when we graph the same differential form with  $\alpha$  on a logarithmic scale, the horizontal measure is now  $d\log\alpha = \frac{d\alpha}{\alpha}$ . Thus we should plot  $\alpha n(\alpha)$ , since the area under this curve is  $\int \alpha n(\alpha)d\log\alpha$ , which is equal to the intended  $\int n(\alpha)d\alpha$ . This is the reason for the extra power of  $\alpha$  that appears in almost all of our figures. When graphing a 2-form such as  $\alpha^{3/2}f_r(\alpha,p)d\alpha \wedge dp$ , shown in Fig. 4, we include both an extra power of  $\alpha$  and  $p$ , since both axes are logarithmic.

Our conjecture that the loop production power is a scaling quantity (even in the absence of gravitational back-reaction) can be phrased in terms of the 1-form  $xf(x)dx$ , where  $x$  is the scaling energy of the loop. Since the integral of a 1-form is a scalar function, we can define scaling of the loop production function to mean the integral  $\mathcal{P}(t,x) = \int_0^x x'f(t,x')dx'$  converges to a time-independent smooth function  $\mathcal{P}(x)$  that vanishes at  $x = 0$ . This means that no power flows into loops of size set by the initial conditions, or any size sufficiently far below the horizon scale.

## 2. The Boltzmann equation

We show how to compute the distribution of loops from their production rate, in the language of differential forms. This is the purpose of a Boltzmann equation (see e.g., Refs. [71–73]), which describes the (non)conservation of some current in phase space. We will consider the phase space to be spanned by the loop’s mass and momentum per unit mass, and so the observable quantity will be the comoving number density, given by the two-form  $n(t,m,p)dm \wedge dp$ , which describes the number of loops per comoving volume at time  $t$  with mass between  $m$  and  $m + dm$ , and with momentum between  $p$  and  $p + dp$ .

Let us first imagine that all loops have the same mass  $M(t)$  and momentum  $P(t)$ , where these functions smoothly vary with time. Further, if the loops are neither created nor destroyed, their constant comoving number density  $n$  is described by the conserved current

$$\mathcal{J} = n\delta(m - M(t))(dm - \dot{M}dt) \wedge \delta(p - P(t))(dp - \dot{P}dt), \quad (\text{A1})$$

where  $\delta$  is the Dirac delta function, and  $\dot{M}(t) = \frac{dM(t)}{dt}$ , etc. Notice that this current can be written

$$\mathcal{J} = nd\Theta(m - M(t)) \wedge d\Theta(p - P(t)), \quad (\text{A2})$$

where  $\Theta$  is the step function. This form of  $\mathcal{J}$  makes it clear that its contour surfaces are parallel to  $(M, P)$ , i.e., the flow generated by  $\dot{M}$  and  $\dot{P}$ . Since  $d^2 \equiv 0$ , the current is indeed conserved:

$$d\mathcal{J} = 0. \quad (\text{A3})$$

We can generalize the above current to have support on more than a single value of  $m$  and  $p$  by adding together many parallel currents. We measure the number density on surfaces of constant  $t$ , so we should define  $n(t,m,p)dm \wedge dp$  as the pullback of  $\mathcal{J}$  onto this surface. (In the above case,  $n(t,m,p) = n\delta(m - M(t))\delta(p - P(t))$ .) Now, the integral curves  $M$  and  $P$  will have two sets of arguments. On the one hand,  $M = M(t')$ , since a given loop’s mass depends only on time. But each integral curve depends only on its starting value, so  $M = M(t'; t, m, p)$ , with  $M(t; t, m, p) = m$ . Notice  $\dot{M}(t, m, p) = \frac{d}{dt'}M(t'; t, m, p)|_{t'=t}$ .

Let us consider a more general two-form  $\mathcal{J}$  which is not necessarily conserved:

$$d\mathcal{J} = \mathcal{F}, \quad (\text{A4})$$

where  $\mathcal{F} = f(t, m, p) dt \wedge dm \wedge dp$  is an arbitrary three-form describing the number of loops per comoving volume that are produced between times  $t$  and  $t + dt$  which have mass between  $m$  and  $m + dm$  and momentum between  $p$  and  $p + dp$ . This is the abstract form of the Boltzmann equation. Even the most general  $\mathcal{J}$  we can consider is not completely arbitrary, but describes a current which flows along the integral curves of the vector field generated by  $\dot{M}(t, m, p)$  and  $\dot{P}(t, m, p)$ , which means we can relate it to  $n(t, m, p)$  by

$$\mathcal{J} = n(t, m, p) \left( dm - \dot{M}(t, m, p) dt \right) \wedge \left( dp - \dot{P}(t, m, p) dt \right), \quad (\text{A5})$$

i.e., this is the unique two-form whose pullback vanishes on surfaces parallel<sup>6</sup> to the flow, and whose pullback on constant time surfaces is given by  $n(t, m, p) dm \wedge dp$ . Thus we can rewrite the Boltzmann equation (A4) as

$$d \left[ n \left( dm - \dot{M} dt \right) \wedge \left( dp - \dot{P} dt \right) \right] = f dt \wedge dm \wedge dp, \quad (\text{A6})$$

from which we can derive the more familiar form<sup>7</sup>

$$\frac{\partial}{\partial t} n(t, m, p) + \frac{\partial}{\partial m} \left( \dot{M}(t, m, p) n(t, m, p) \right) + \frac{\partial}{\partial p} \left( \dot{P}(t, m, p) n(t, m, p) \right) = f(t, m, p). \quad (\text{A7})$$

This form of the Boltzmann equation would be useful for determining  $f$ , given  $n$ . We are interested in finding  $n(t, m, p)$  for a given  $f(t, m, p)$ , which can be done using Stokes' theorem, which says

$$\int_B \mathcal{F} = \int_B d\mathcal{J} = \int_{\partial B} \mathcal{J}, \quad (\text{A8})$$

where the last integral will contain the term  $n(t, m, p) dm \wedge dp$  if we choose  $B$  properly. Thus we will find  $n(t, m, p)$  by integrating the abstract Boltzmann equation, but along a specially chosen infinitesimally narrow volume. Imagine drawing a narrow three dimensional pill box  $B$  in extended phase space which begins at some initial time  $t_i$ , and ends at the time we are interested in,  $t$ . The pill box intersects the  $t$ -surface to form an infinitesimal parallelogram centered at  $(m, p)$  with sides  $dm$  and  $dp$ . We assume the initial boundary data  $n(t_i, m, p)$  are known for some  $t_i$ . Finally, we will choose the four long sides of the pill box to follow the flow in phase space generated by  $\dot{M}$  and  $\dot{P}$ . By doing this, we have ensured that in Eq. (A8), the integral of  $\mathcal{J}$  over the boundary of the pill box will vanish on four out of six sides, and so the bulk integral of  $\mathcal{F}$  over  $B$  will give us  $n(t, m, p)$  in terms of  $f$  and the initial boundary data  $n(t_i, m, p)$ . We illustrate  $B$  in Fig. 15 below.

### 3. The flow $(M, P)$

To use the Boltzmann equation, we must know what generates the flow, i.e., given any values for the mass and momentum  $m, p$  at time  $t$ , we must know the rate at which they

<sup>6</sup> In other words,  $\mathcal{J}_{\mu\nu} \mathcal{V}^\nu = 0$ , where  $\mathcal{V} = \frac{\partial}{\partial t} + \dot{M} \frac{\partial}{\partial m} + \dot{P} \frac{\partial}{\partial p}$ .

<sup>7</sup> Notice since  $n$  is not a scalar, the following is *not* correct:  $f = \frac{d}{dt} n = \frac{\partial}{\partial t} n + \dot{M} \frac{\partial}{\partial m} n + \dot{P} \frac{\partial}{\partial p} n$ . The missing term  $n \frac{\partial}{\partial p} \dot{P}$  is important; Even for  $f = 0$ , as loop momenta redshift, the peak value of  $n$  grows to compensate its shrinking support.

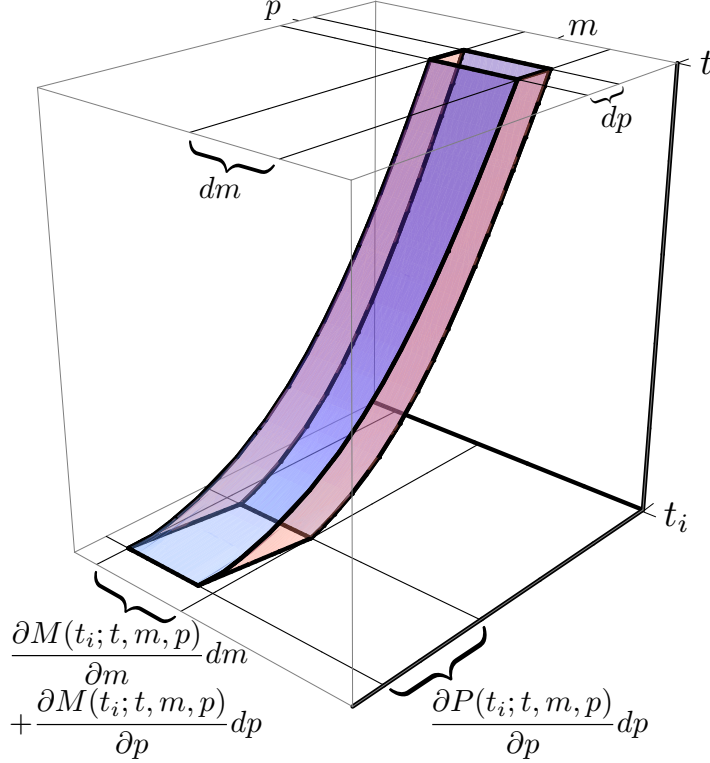


FIG. 15. The pill box  $B$ . The boundary  $\partial B$  consists of six faces, the four curved of which do not contribute to  $\int \mathcal{J}$ . The top and bottom parallelograms do contribute and have areas given by  $dm \wedge dp$  and  $\left( \frac{\partial M_i}{\partial m} \frac{\partial P_i}{\partial p} - \frac{\partial M_i}{\partial p} \frac{\partial P_i}{\partial m} \right) dm \wedge dp$ , respectively.

change,  $\dot{M}(t, m, p)$ ,  $\dot{P}(t, m, p)$ . These functions define a vector field  $\mathcal{V}$  on extended phase space,

$$\mathcal{V} = \frac{\partial}{\partial t} + \dot{M} \frac{\partial}{\partial m} + \dot{P} \frac{\partial}{\partial p}. \quad (\text{A9})$$

We can characterize the associated integral curves with the functions  $M' = M(t'; t, m, p)$  and  $P' = P(t'; t, m, p)$ . These determine the entire trajectory as a function of  $t'$ , given the initial starting point  $(m, p)$  at time  $t$ . We solve an autonomous system of ordinary differential equations to get from the generators  $\dot{M}$  and  $\dot{P}$  to the curves  $M'$  and  $P'$ , and so the solution is unique<sup>8</sup>.

#### 4. The solution

We are now ready to solve for  $n(t, m, p)$  by integrating the Boltzmann equation along the narrow pill box  $B$ . The top face of  $B$  is denoted  $B \cap t$  and is a tiny parallelogram of area  $dm \wedge dp$ . The bottom face is a parallelogram denoted  $B \cap t_i$  and has area given by the Jacobian determinant

$$\left| \frac{\partial (M_i, P_i)}{\partial (m, p)} \right| dm \wedge dp = \left( \frac{\partial M_i}{\partial m} \frac{\partial P_i}{\partial p} - \frac{\partial M_i}{\partial p} \frac{\partial P_i}{\partial m} \right) dm \wedge dp. \quad (\text{A10})$$

<sup>8</sup> See [74] for a review of flows.

The remaining four faces contribute nothing in Eq. (A8). Using Stokes' theorem,

$$n(t, m, p)dm \wedge dp = \int_{B \cap t} \mathcal{J}, \quad (\text{A11})$$

$$= \int_B \mathcal{F} + \int_{B \cap t_i} \mathcal{J}, \quad (\text{A12})$$

$$= \left[ \int_{t_i}^t f(t', M(t'; t, m, p), P(t'; t, m, p)) \left| \frac{\partial(M(t'), P(t'))}{\partial(m, p)} \right| dt' \right. \\ \left. + n(t_i, M(t_i; t, m, p), P(t_i; t, m, p)) \left| \frac{\partial(M(t_i), P(t_i))}{\partial(m, p)} \right| \right] dm \wedge dp, \quad (\text{A13})$$

or

$$n(t, m, p) = n(t_i, M_i, P_i) \left| \frac{\partial(M_i, P_i)}{\partial(m, p)} \right| + \int_{t_i}^t f(t', M', P') \left| \frac{\partial(M', P')}{\partial(m, p)} \right| dt'. \quad (\text{A14})$$

Notice we have defined the integral curves  $M(t')$  and  $P(t')$  by integrating  $\dot{M}$  and  $\dot{P}$  from the final surface  $t$  backward as a function of  $t'$ . This enabled us to keep explicit dependence on  $m$  and  $p$ . We must account for the fact that the pill box cross-sectional area changes by a factor of the Jacobian determinant, as shown in Fig. 15. In our approximation, because the momentum of a loop redshifts without any regard for the value of the mass, the Jacobian determinant has one term,  $\frac{\partial M}{\partial m} \frac{\partial P}{\partial p}$ .

## Appendix B: The exact flow

Here we give the solution to the flow  $(M, P)$  for arbitrary loop momentum per unit mass  $p$ . The time derivatives which generate the flow are given by

$$\dot{M} = -\Gamma G \mu^2 / \gamma, \quad (\text{B1})$$

$$\dot{P} = -\frac{\dot{a}}{a} P, \quad (\text{B2})$$

where  $\gamma = 1/\sqrt{1-v^2} = \sqrt{p^2+1}$  is the time-dilation factor.

Changing to redshift as a time variable, the solution for  $P$  is just

$$P' = P(z'; z, m, p) = p \frac{1+z'}{1+z}, \quad (\text{B3})$$

as before. The loop mass obeys

$$M' = M(z'; z, m, p) = -\Gamma G \mu^2 \int \frac{1}{\gamma'} \frac{dt'}{dz'} dz' = \Gamma G \mu^2 \int \frac{1}{(1+z')H(z')\gamma'} dz', \quad (\text{B4})$$

where

$$\gamma' = \sqrt{P'^2 + 1}, \quad (\text{B5})$$

If we neglect dark energy, we can write

$$H(z) = H_0 \sqrt{\Omega_{m,0} (1+z)^3 \left( 1 + \frac{1+z}{1+z_{\text{eq}}} \right)}, \quad (\text{B6})$$

which makes it possible to perform the integral in Eq. (B4) in closed form, but the result in terms of elliptic integrals is not very enlightening.

### Appendix C: Tiny, recent loops

We assumed above that long strings are smoothed by gravitational back reaction at scales  $\Gamma G\mu t$ , and thus that no loops are produced at time  $t$  with  $\alpha \ll \Gamma G\mu t$ . If this is not the case, we can have a different situation. Loops formed recently with size  $\alpha > \Gamma G\mu$  are always dominated by loops formed long ago, when the string network was denser. But when  $\alpha \ll \Gamma G\mu$ , the possible formation time for a loop that currently has size  $\alpha$  no longer decreases with  $\alpha$ , because loops from too long ago have evaporated. This raises the possibility, which we investigate in this appendix, that such tiny loops are mainly of recent origin.

Thus we consider a second population of loops created with  $\alpha \ll \Gamma G\mu$ . Such loops live for much less than a Hubble time, so for them we can neglect redshifting and increase in  $t$  from formation to observation. Thus we set  $a(t') = a(t)$ ,  $d_h(t') = d_h(t)$ , and  $P' = p$  in Eq. (9) to get

$$n_{\text{recent}}(\alpha, p) = \int_0^t \frac{1}{d_h} f(\alpha + \Gamma G\mu(t - t')/\gamma, p) dt' \quad (\text{C1})$$

where  $\gamma = \sqrt{p^2 + 1} \sim p$  is the Lorentz boost of a loop with momentum  $p$ . Changing variables, we find

$$n_{\text{recent}}(\alpha, p) = \frac{\gamma}{\Gamma G\mu} \int_\alpha^\infty f(\alpha', p) d\alpha' \quad (\text{C2})$$

If we are not concerned with loop velocities, we can approximate

$$n_{\text{recent}}(\alpha) = \frac{1}{\Gamma G\mu} \int_\alpha^\infty \gamma(\alpha') f(\alpha') d\alpha' \quad (\text{C3})$$

where  $\gamma(\alpha')$  denotes the average boost with which loops of mass  $\alpha'$  are emitted. The production rate  $f(\alpha')$  increases more quickly than  $1/\alpha'$  as  $\alpha'$  decreases, until reaching some cutoff due to gravitational smoothing of the long-string network. The cutoff is given by the shortest-wavelength wiggles that have survived gravitational damping. If this wavelength were  $\Gamma G\mu t$ , the population of recent loops would be of no consequence. But Ref. [75] argued that short-wavelength structures on long strings will be damped slowly, because they are only able to interact with wiggles of similar wavelengths, so we will consider a cutoff

$$\lambda_{\text{min}} \sim (\Gamma G\mu)^\delta t \quad (\text{C4})$$

which gives a limit

$$x_{\text{min}} \sim (\Gamma G\mu)^\delta \quad (\text{C5})$$

According to Ref. [75], the smallest scales depend on the falloff of the amplitude of structures on the string with decreasing wavelength  $\lambda$ . But since strings have kinks, the amplitude-to-wavelength ratio of the Fourier components must fall no more rapidly than  $\lambda$ , which implies<sup>9</sup>  $\delta \geq 3/2$ .

Below  $\alpha = \alpha_{\text{min}}$ ,  $n_{\text{recent}}$  is a constant

$$n_{\text{recent}}(0) = \frac{1}{\Gamma G\mu} \int_{\alpha_{\text{min}}}^\infty \gamma(\alpha') f(\alpha') d\alpha' \quad (\text{C6})$$

---

<sup>9</sup> Ref. [75] gave a model with  $\delta = 5/2$  in the matter era, but this model assumed no intercommutations and thus no kinks.

If we take a model in which the formation of loops with  $x_{\min} < x \ll \Gamma G\mu$  is given by

$$f(x) = cx^{-\beta} \quad (\text{C7})$$

and all loops of size  $x$  have boost

$$\gamma(x) = c'x^{-\kappa} \quad (\text{C8})$$

and thus  $\alpha(x) = x^{1+\kappa}/c'$ . Then

$$n_{\text{recent}}(0) = \frac{1}{\Gamma G\mu} \int_{x_{\min}}^{\infty} \gamma(x)f(x)dx' = \frac{cc'}{\Gamma G\mu(\beta + \kappa - 1)x_{\min}^{\beta+\kappa-1}} \quad (\text{C9})$$

$$= \frac{cc'}{(\beta + \kappa - 1)(\Gamma G\mu)^{1+(\beta+\kappa-1)\delta}} \quad (\text{C10})$$

For small  $\alpha$ , Eq. (15) also gives a constant  $n(\alpha)$  as  $\alpha \rightarrow 0$ . The ratio of recently produced tiny loops to old tiny loops is

$$\frac{n_{\text{recent}}(0)}{n(0)} = \frac{cc'}{(1-\nu)(\beta + \kappa - 1)} \frac{(\Gamma G\mu)^{3-3\nu-(\beta+\kappa-1)\delta}}{\int_0^{\infty} \alpha'^{3-3\nu} f(\alpha') d\alpha'} \quad (\text{C11})$$

In the radiation era, fits to simulation data give

$$f(x) \approx 1.64x^{-1.97} \quad (\text{C12})$$

$$\gamma(x) \approx 0.50x^{-0.21} \quad (\text{C13})$$

which with  $\delta = 3/2$  give

$$\frac{n_{\text{recent}}(0)}{n_r(0)} = 1.64(\Gamma G\mu)^{-0.27} \quad (\text{C14})$$

In the matter era, we find

$$f(x) \approx 3.40x^{-1.78} \quad (\text{C15})$$

$$\gamma(x) \approx 0.40x^{-0.30} \quad (\text{C16})$$

which give

$$\frac{n_{\text{recent}}(0)}{n_m(0)} = 4.4(\Gamma G\mu)^{-0.62} \quad (\text{C17})$$

Since  $\Gamma G\mu \ll 1$ , the negative exponents imply that most tiny loops are recently produced.

The total number density of recently-produced loops with  $x < \Gamma G\mu$  is

$$n_{\text{recent}} = \int_0^{\Gamma G\mu} dx x f(x) = \frac{c(\Gamma G\mu)^{1-\beta}}{2-\beta}. \quad (\text{C18})$$

In the radiation era,

$$n_{\text{recent}} \approx 54(\Gamma G\mu)^{-0.97}, \quad (\text{C19})$$

which is much smaller than the density of old loops given by Eq. (19). In the matter era,

$$n_{\text{recent}} \approx 16(\Gamma G\mu)^{-0.78}. \quad (\text{C20})$$

For  $\Gamma G\mu < 10^{-6}$ , this is no more than 1/8 of the number of old loops given by Eq. (32). If one considers loop energies, the recent loops make an even smaller contribution.

- 
- [1] A. Vilenkin, “Gravitational radiation from cosmic strings,” *Phys.Lett.* **B107**, 47–50 (1981).
  - [2] C.J. Hogan and M.J. Rees, “Gravitational interactions of cosmic strings,” *Nature* **311**, 109–113 (1984).
  - [3] Tanmay Vachaspati and Alexander Vilenkin, “Gravitational Radiation from Cosmic Strings,” *Phys.Rev.* **D31**, 3052 (1985).
  - [4] Frank S. Accetta and Lawrence M. Krauss, “The stochastic gravitational wave spectrum resulting from cosmic string evolution,” *Nucl.Phys.* **B319**, 747 (1989).
  - [5] David P. Bennett and Francois R. Bouchet, “Constraints on the gravity wave background generated by cosmic strings,” *Phys.Rev.* **D43**, 2733–2735 (1991).
  - [6] R.R. Caldwell and Bruce Allen, “Cosmological constraints on cosmic string gravitational radiation,” *Phys.Rev.* **D45**, 3447–3468 (1992).
  - [7] Xavier Siemens, Vuk Mandic, and Jolien Creighton, “Gravitational wave stochastic background from cosmic (super)strings,” *Phys.Rev.Lett.* **98**, 111101 (2007), arXiv:astro-ph/0610920 [astro-ph].
  - [8] Matthew R. DePies and Craig J. Hogan, “Stochastic Gravitational Wave Background from Light Cosmic Strings,” *Phys.Rev.* **D75**, 125006 (2007), arXiv:astro-ph/0702335 [astro-ph].
  - [9] S. Olmez, V. Mandic, and X. Siemens, “Gravitational-Wave Stochastic Background from Kinks and Cusps on Cosmic Strings,” *Phys.Rev.* **D81**, 104028 (2010), arXiv:1004.0890 [astro-ph.CO].
  - [10] S.A. Sanidas, R.A. Battye, and B.W. Stappers, “Constraints on cosmic string tension imposed by the limit on the stochastic gravitational wave background from the European Pulsar Timing Array,” *Phys.Rev.* **D85**, 122003 (2012), arXiv:1201.2419 [astro-ph.CO].
  - [11] Sotirios A. Sanidas, Richard A. Battye, and Benjamin W. Stappers, “Projected constraints on the cosmic (super)string tension with future gravitational wave detection experiments,” *Astrophys.J.* **764**, 108 (2013), arXiv:1211.5042 [astro-ph.CO].
  - [12] Pierre Binétruy, Alejandro Bohe, Chiara Caprini, and Jean-Francois Dufaux, “Cosmological Backgrounds of Gravitational Waves and eLISA/NGO: Phase Transitions, Cosmic Strings and Other Sources,” *JCAP* **1206**, 027 (2012), arXiv:1201.0983 [gr-qc].
  - [13] Sachiko Kuroyanagi, Koichi Miyamoto, Toyokazu Sekiguchi, Keitaro Takahashi, and Joseph Silk, “Forecast constraints on cosmic string parameters from gravitational wave direct detection experiments,” *Phys.Rev.* **D86**, 023503 (2012), arXiv:1202.3032 [astro-ph.CO].
  - [14] Sachiko Kuroyanagi, Koichi Miyamoto, Toyokazu Sekiguchi, Keitaro Takahashi, and Joseph Silk, “Forecast constraints on cosmic strings from future CMB, pulsar timing and gravitational wave direct detection experiments,” *Phys.Rev.* **D87**, 023522 (2013), arXiv:1210.2829 [astro-ph.CO].
  - [15] Thibault Damour and Alexander Vilenkin, “Gravitational wave bursts from cosmic strings,” *Phys.Rev.Lett.* **85**, 3761–3764 (2000), arXiv:gr-qc/0004075 [gr-qc].
  - [16] Thibault Damour and Alexander Vilenkin, “Gravitational wave bursts from cusps and kinks on cosmic strings,” *Phys.Rev.* **D64**, 064008 (2001), arXiv:gr-qc/0104026 [gr-qc].
  - [17] Thibault Damour and Alexander Vilenkin, “Gravitational radiation from cosmic (super)strings: Bursts, stochastic background, and observational windows,” *Phys.Rev.* **D71**,

- 063510 (2005), arXiv:hep-th/0410222 [hep-th].
- [18] Xavier Siemens, Jolien Creighton, Irit Maor, Saikat Ray Majumder, Kipp Cannon, *et al.*, “Gravitational wave bursts from cosmic (super)strings: Quantitative analysis and constraints,” *Phys.Rev.* **D73**, 105001 (2006), arXiv:gr-qc/0603115 [gr-qc].
  - [19] Craig J. Hogan, “Gravitational Waves from Light Cosmic Strings: Backgrounds and Bursts with Large Loops,” *Phys.Rev.* **D74**, 043526 (2006), arXiv:astro-ph/0605567 [astro-ph].
  - [20] Tania Regimbau, Stefanos Giampanis, Xavier Siemens, and Vuk Mandic, “The stochastic background from cosmic (super)strings: popcorn and (Gaussian) continuous regimes,” *Phys.Rev.* **D85**, 066001 (2012), arXiv:1111.6638 [astro-ph.CO].
  - [21] Ken D. Olum and Alexander Vilenkin, “Reionization from cosmic string loops,” *Phys.Rev.* **D74**, 063516 (2006), arXiv:astro-ph/0605465 [astro-ph].
  - [22] Benjamin Shlaer, Alexander Vilenkin, and Abraham Loeb, “Early structure formation from cosmic string loops,” *JCAP* **1205**, 026 (2012), arXiv:1202.1346 [astro-ph.CO].
  - [23] Michael Pagano and Robert Brandenberger, “The 21cm Signature of a Cosmic String Loop,” *JCAP* **1205**, 014 (2012), arXiv:1201.5695 [astro-ph.CO].
  - [24] Hiroyuki Tashiro, “21 cm Angular Spectrum of Cosmic String Loops,” *Phys.Rev.* **D87**, 123535 (2013), arXiv:1305.4779 [astro-ph.CO].
  - [25] V.S. Berezhinsky, V.I. Dokuchaev, and Yu.N. Eroshenko, “Dense DM clumps seeded by cosmic string loops and DM annihilation,” *JCAP* **1112**, 007 (2011), arXiv:1107.2751 [astro-ph.HE].
  - [26] David F. Chernoff and S.H. Henry Tye, “Cosmic String Detection via Microlensing of Stars,” (2007), arXiv:0709.1139 [astro-ph].
  - [27] David F. Chernoff, “Clustering of Superstring Loops,” (2009), arXiv:0908.4077 [astro-ph.CO].
  - [28] M.S. Pshirkov and A.V. Tutstov, “Local constraints on cosmic string loops from photometry and pulsar timing,” *Phys.Rev.* **D81**, 083519 (2010), arXiv:0911.4955 [astro-ph.CO].
  - [29] Diana Battefeld, Thorsten Battefeld, Daniel H. Wesley, and Mark Wyman, “Magnetogenesis from Cosmic String Loops,” *JCAP* **0802**, 001 (2008), arXiv:0708.2901 [astro-ph].
  - [30] Robert H. Brandenberger, “On the Decay of Cosmic String Loops,” *Nucl.Phys.* **B293**, 812 (1987).
  - [31] Jane H. MacGibbon and Robert H. Brandenberger, “High-energy neutrino flux from ordinary cosmic strings,” *Nucl.Phys.* **B331**, 153 (1990).
  - [32] M. Mohazzab, “CUSP annihilation on ordinary cosmic strings,” *Int.J.Mod.Phys.* **D3**, 493–498 (1994), arXiv:hep-ph/9307286 [hep-ph].
  - [33] J.J. Blanco-Pillado and Ken D. Olum, “The Form of cosmic string cusps,” *Phys.Rev.* **D59**, 063508 (1999), arXiv:gr-qc/9810005 [gr-qc].
  - [34] Ken D. Olum and J.J. Blanco-Pillado, “Field theory simulation of Abelian Higgs cosmic string cusps,” *Phys.Rev.* **D60**, 023503 (1999), arXiv:gr-qc/9812040 [gr-qc].
  - [35] Veniamin Berezhinsky, Eray Sabancilar, and Alexander Vilenkin, “Extremely High Energy Neutrinos from Cosmic Strings,” *Phys.Rev.* **D84**, 085006 (2011), arXiv:1108.2509 [astro-ph.CO].
  - [36] Christopher T. Hill, David N. Schramm, and Terry P. Walker, “Ultrahigh-Energy Cosmic Rays from Superconducting Cosmic Strings,” *Phys.Rev.* **D36**, 1007 (1987).
  - [37] Veniamin Berezhinsky, Ken D. Olum, Eray Sabancilar, and Alexander Vilenkin, “UHE neutrinos from superconducting cosmic strings,” *Phys.Rev.* **D80**, 023014 (2009), arXiv:0901.0527 [astro-ph.HE].
  - [38] Tanmay Vachaspati, “Cosmic Sparks from Superconducting Strings,” *Phys.Rev.Lett.* **101**, 141301 (2008), arXiv:0802.0711 [astro-ph].



- [39] Yi-Fu Cai, Eray Sabancilar, and Tanmay Vachaspati, “Radio bursts from superconducting strings,” *Phys.Rev.* **D85**, 023530 (2012), arXiv:1110.1631 [astro-ph.CO].
- [40] Yi-Fu Cai, Eray Sabancilar, Daniele A. Steer, and Tanmay Vachaspati, “Radio Broadcasts from Superconducting Strings,” *Phys.Rev.* **D86**, 043521 (2012), arXiv:1205.3170 [astro-ph.CO].
- [41] Mark Srednicki and Stefan Theisen, “Nongravitational Decay of Cosmic Strings,” *Phys.Lett.* **B189**, 397 (1987).
- [42] Thibault Damour and Alexander Vilenkin, “Cosmic strings and the string dilaton,” *Phys.Rev.Lett.* **78**, 2288–2291 (1997), arXiv:gr-qc/9610005 [gr-qc].
- [43] Marco Peloso and Lorenzo Sorbo, “Moduli from cosmic strings,” *Nucl.Phys.* **B649**, 88–100 (2003), arXiv:hep-ph/0205063 [hep-ph].
- [44] E. Babichev and M. Kachelriess, “Constraining cosmic superstrings with dilaton emission,” *Phys.Lett.* **B614**, 1–6 (2005), arXiv:hep-th/0502135 [hep-th].
- [45] Tanmay Vachaspati, “Cosmic Rays from Cosmic Strings with Condensates,” *Phys.Rev.* **D81**, 043531 (2010), arXiv:0911.2655 [astro-ph.CO].
- [46] Jean-Francois Dufaux, “Cosmic Super-Strings and Kaluza-Klein Modes,” *JCAP* **1209**, 022 (2012), arXiv:1201.4850 [hep-th].
- [47] Cecilia Lunardini and Eray Sabancilar, “Cosmic Strings as Emitters of Extremely High Energy Neutrinos,” *Phys.Rev.* **D86**, 085008 (2012), arXiv:1206.2924 [astro-ph.CO].
- [48] Jose J. Blanco-Pillado, Ken D. Olum, and Benjamin Shlaer, “Large parallel cosmic string simulations: New results on loop production,” *Phys.Rev.* **D83**, 083514 (2011), arXiv:1101.5173 [astro-ph.CO].
- [49] Jose J. Blanco-Pillado, Ken D. Olum, and Benjamin Shlaer, “A new parallel simulation technique,” *J.Comput.Phys.* **231**, 98–108 (2012), arXiv:1011.4046 [physics.comp-ph].
- [50] Andreas Albrecht and N. Turok, “Evolution of Cosmic Strings,” *Phys.Rev.Lett.* **54**, 1868–1871 (1985).
- [51] Andreas Albrecht and Neil Turok, “Evolution of Cosmic String Networks,” *Phys.Rev.* **D40**, 973–1001 (1989).
- [52] David P. Bennett and Francois R. Bouchet, “Evidence for a Scaling Solution in Cosmic String Evolution,” *Phys.Rev.Lett.* **60**, 257 (1988).
- [53] David P. Bennett and Francois R. Bouchet, “Cosmic string evolution,” *Phys.Rev.Lett.* **63**, 2776 (1989).
- [54] David P. Bennett and Francois R. Bouchet, “High resolution simulations of cosmic string evolution. 1. Network evolution,” *Phys.Rev.* **D41**, 2408 (1990).
- [55] Bruce Allen and E.P.S. Shellard, “Cosmic string evolution: a numerical simulation,” *Phys.Rev.Lett.* **64**, 119–122 (1990).
- [56] Vitaly Vanchurin, Ken Olum, and Alexander Vilenkin, “Cosmic string scaling in flat space,” *Phys.Rev.* **D72**, 063514 (2005), arXiv:gr-qc/0501040 [gr-qc].
- [57] Christophe Ringeval, Mairi Sakellariadou, and Francois Bouchet, “Cosmological evolution of cosmic string loops,” *JCAP* **0702**, 023 (2007), arXiv:astro-ph/0511646 [astro-ph].
- [58] Vitaly Vanchurin, Ken D. Olum, and Alexander Vilenkin, “Scaling of cosmic string loops,” *Phys.Rev.* **D74**, 063527 (2006), arXiv:gr-qc/0511159 [gr-qc].
- [59] Ken D. Olum and Vitaly Vanchurin, “Cosmic string loops in the expanding Universe,” *Phys.Rev.* **D75**, 063521 (2007), arXiv:astro-ph/0610419 [astro-ph].
- [60] Larissa Lorenz, Christophe Ringeval, and Mairi Sakellariadou, “Cosmic string loop distribution on all length scales and at any redshift,” *JCAP* **1010**, 003 (2010), arXiv:1006.0931

- [astro-ph.CO].
- [61] Joseph Polchinski and Jorge V. Rocha, “Analytic study of small scale structure on cosmic strings,” *Phys.Rev.* **D74**, 083504 (2006), arXiv:hep-ph/0606205 [hep-ph].
  - [62] C.J.A.P. Martins and E.P.S. Shellard, “Fractal properties and small-scale structure of cosmic string networks,” *Phys.Rev.* **D73**, 043515 (2006), arXiv:astro-ph/0511792 [astro-ph].
  - [63] Florian Dubath, Joseph Polchinski, and Jorge V. Rocha, “Cosmic String Loops, Large and Small,” *Phys.Rev.* **D77**, 123528 (2008), arXiv:0711.0994 [astro-ph].
  - [64] P.A.R. Ade *et al.* (Planck Collaboration), “Planck 2013 results. XVI. Cosmological parameters,” (2013), arXiv:1303.5076 [astro-ph.CO].
  - [65] Pau Amaro-Seoane, Sofiane Aoudia, Stanislav Babak, Pierre Binetruy, Emanuele Berti, *et al.*, “Low-frequency gravitational-wave science with eLISA/NGO,” *Class.Quant.Grav.* **29**, 124016 (2012), arXiv:1202.0839 [gr-qc].
  - [66] B.P. Abbott *et al.* (LIGO Scientific Collaboration), “First LIGO search for gravitational wave bursts from cosmic (super)strings,” *Phys.Rev.* **D80**, 062002 (2009), arXiv:0904.4718 [astro-ph.CO].
  - [67] R. van Haasteren, Y. Levin, G.H. Janssen, K. Lazaridis, M. Kramer, *et al.*, “Placing limits on the stochastic gravitational-wave background using European Pulsar Timing Array data,” *Mon.Not.Roy.Astron.Soc.* **414**, 3117–3128 (2011), arXiv:1103.0576 [astro-ph.CO].
  - [68] P.B. Demorest, R.D. Ferdman, M.E. Gonzalez, D. Nice, S. Ransom, *et al.*, “Limits on the Stochastic Gravitational Wave Background from the North American Nanohertz Observatory for Gravitational Waves,” *Astrophys.J.* **762**, 94 (2013), arXiv:1201.6641 [astro-ph.CO].
  - [69] Hassan Firouzjahi and S.-H. Henry Tye, “Brane inflation and cosmic string tension in superstring theory,” *JCAP* **0503**, 009 (2005), arXiv:hep-th/0501099 [hep-th].
  - [70] A. Vilenkin and E. P. S. Shellard, *Cosmic Strings and other Topological Defects* (Cambridge University Press, Cambridge, 2000).
  - [71] Edmund J. Copeland, T.W.B. Kibble, and Daniele A. Steer, “The Evolution of a network of cosmic string loops,” *Phys.Rev.* **D58**, 043508 (1998), arXiv:hep-ph/9803414 [hep-ph].
  - [72] Louis Leblond, Benjamin Shlaer, and Xavier Siemens, “Gravitational Waves from Broken Cosmic Strings: The Bursts and the Beads,” *Phys.Rev.* **D79**, 123519 (2009), arXiv:0903.4686 [astro-ph.CO].
  - [73] Patrick Peter and Christophe Ringeval, “A Boltzmann treatment for the vorton excess problem,” *JCAP* **1305**, 005 (2013), arXiv:1302.0953 [astro-ph.CO].
  - [74] M. Nakahara, *Geometry, topology and physics* (Hilger, Bristol, UK, 1990).
  - [75] Xavier Siemens, Ken D. Olum, and Alexander Vilenkin, “On the size of the smallest scales in cosmic string networks,” *Phys.Rev.* **D66**, 043501 (2002), arXiv:gr-qc/0203006 [gr-qc].